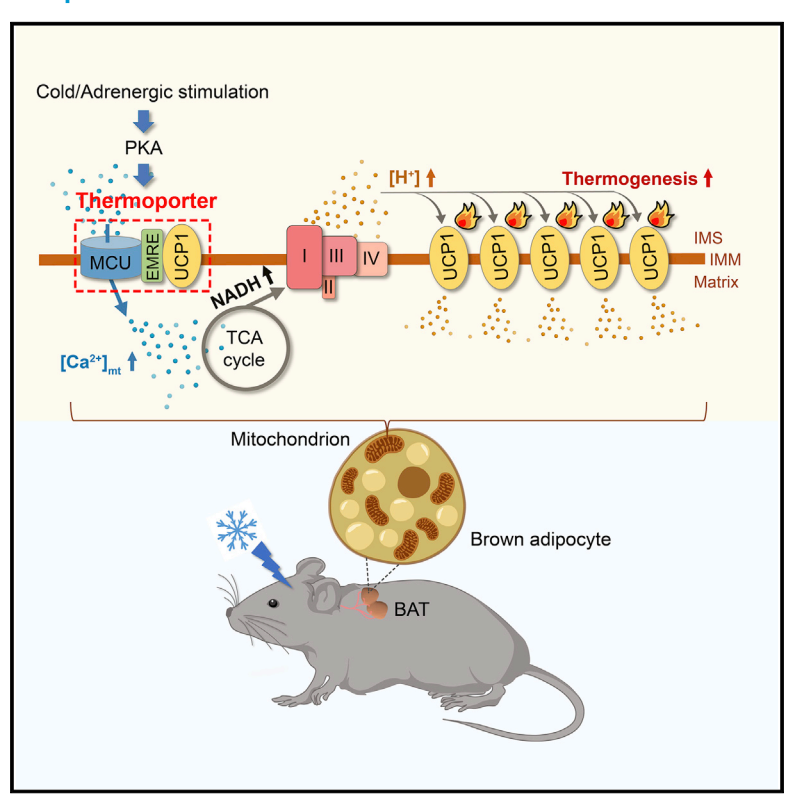
# The mitochondrial calcium uniporter engages UCP1 to form a thermoporter that promotes thermogenesis

# **Graphical abstract**



# **Authors**

Kaili Xue, Dongmei Wu, Yushuang Wang, ..., Zhao Zhou, Zihao Wang, Yifu Qiu

# Correspondence

yifu.qiu@pku.edu.cn

# In brief

Xue et al. identify an MCU-EMRE-UCP1 complex, named thermoporter, in adaptive thermogenesis. Adrenergic-stimulated thermoporter assembly enhances mitochondrial calcium uptake and proton supply, which promotes thermogenesis. The deletion of *Mcu* or *Emre* in brown adipocytes impairs thermogenesis and exacerbates obesity and metabolic dysfunction, whereas enhanced thermoporter assembly results in the opposite phenotypes.

# **Highlights**

- MCU-EMRE and UCP1 form a complex in brown adipocytes upon adrenergic stimulation
- The complex acts as a "thermoporter" that enhances proton supply to promote thermogenesis
- Enhanced thermoporter assembly ameliorates diet-induced obesity and metabolic dysfunction







# **Article**

# The mitochondrial calcium uniporter engages UCP1 to form a thermoporter that promotes thermogenesis

Kaili Xue,¹ Dongmei Wu,¹,² Yushuang Wang,¹ Yiheng Zhao,¹,²,³ Hongyu Shen,¹,²,³ Jingfei Yao,¹ Xun Huang,¹,²,³ Xinmeng Li,¹ Zhao Zhou,¹ Zihao Wang,¹ and Yifu Qiu¹,²,4,\*

<sup>1</sup>Institute of Molecular Medicine, Beijing Key Laboratory of Cardiometabolic Molecular Medicine, College of Future Technology, Peking University, Beijing 100871, China

<sup>2</sup>Peking-Tsinghua Center for Life Sciences, Peking University, Beijing 100871, China

<sup>3</sup>Academy for Advanced Interdisciplinary Studies, Peking University, Beijing 100871, China

<sup>4</sup>Lead contact

\*Correspondence: yifu.qiu@pku.edu.cn https://doi.org/10.1016/j.cmet.2022.07.011

#### **SUMMARY**

Uncoupling protein 1 (UCP1)-mediated adaptive thermogenesis protects mammals against hypothermia and metabolic dysregulation. Whether and how mitochondrial calcium regulates this process remains unclear. Here, we show that mitochondrial calcium uniporter (MCU) recruits UCP1 through essential MCU regulator (EMRE) to form an MCU-EMRE-UCP1 complex upon adrenergic stimulation. This complex formation increases mitochondrial calcium uptake to accelerate the tricarboxylic acid cycle and supply more protons that promote uncoupled respiration, functioning as a thermogenic uniporter. Mitochondrial calcium uptake 1 (MICU1) negatively regulates thermogenesis probably through inhibiting thermogenic uniporter formation. Accordingly, the deletion of *Mcu* or *Emre* in brown adipocytes markedly impairs thermogenesis and exacerbates obesity and metabolic dysfunction. Remarkably, the enhanced assembly of the thermogenic uniporter via *Micu1* knockout or expressing linked EMRE-UCP1 results in opposite phenotypes. Thus, we have uncovered a "thermoporter" that provides a driving force for the UCP1 operation in thermogenesis, which could be leveraged to combat obesity and associated metabolic disorders.

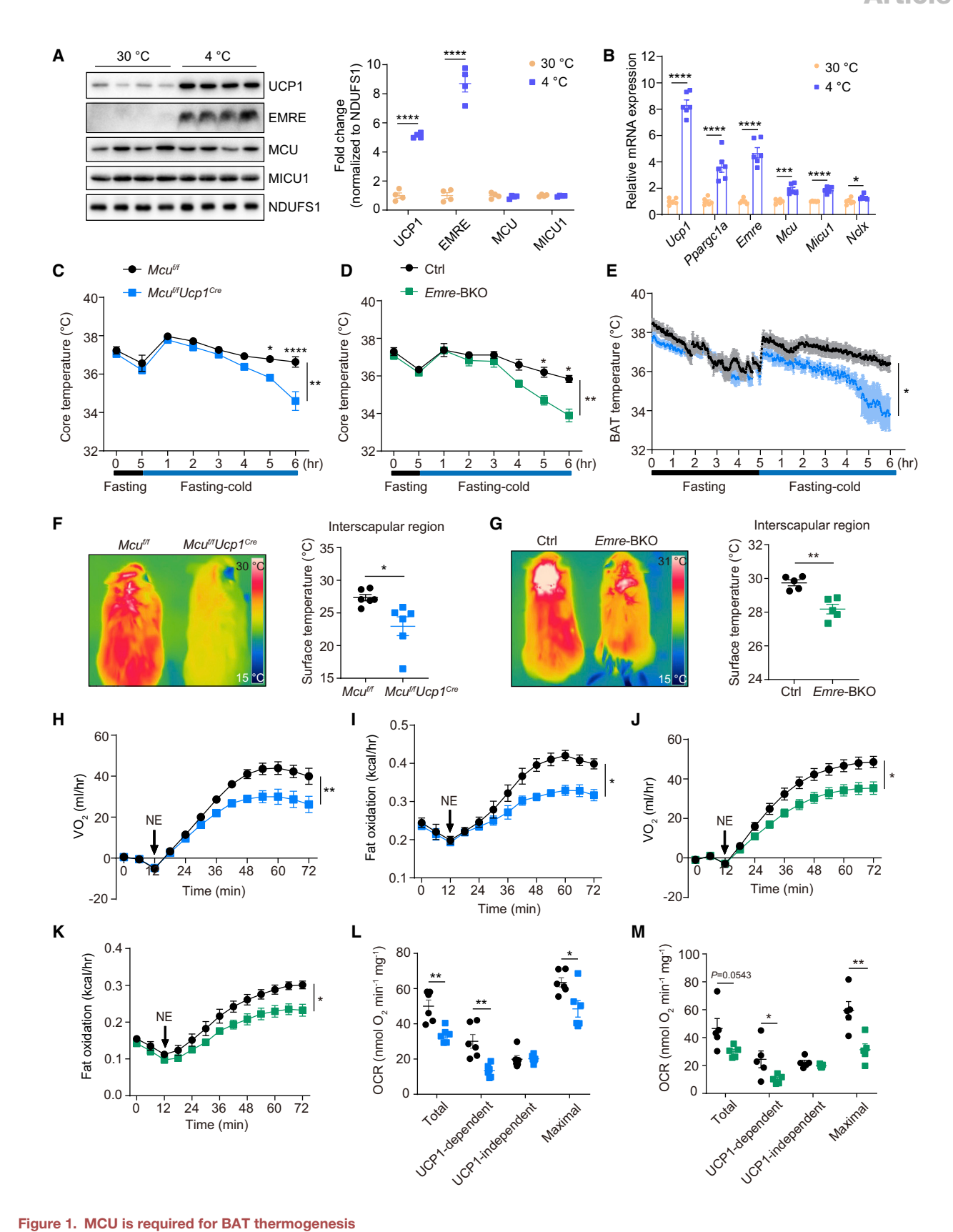
# INTRODUCTION

Obesity and overweight have been globally prevalent in children and adults (Ng et al., 2014). The prevention and treatment of obesity are of great importance since it is closely linked to many major chronic diseases such as cardiovascular diseases, type 2 diabetes, and certain types of cancers (Cao, 2010; Heymsfield and Wadden, 2017). At the organismal level, two fundamental ways can be exploited to combat obesity: to decrease energy/food intake or to increase energy expenditure. Most strategies targeting energy/food intake were to prove unsuccessful as they gave rise to cardiovascular or even psychiatric side effects (Dietrich and Horvath, 2012). Thus, tremendous efforts have been focused on finding ways to increase energy expenditure through adaptive thermogenesis in BAT, where uncoupling protein 1 (UCP1) plays a central role (Cannon and Nedergaard, 2004; Harms and Seale, 2013). UCP1 mediates adaptive thermogenesis by uncoupling oxidative phosphorylation from ATP synthesis and thereby dissipating energy as heat, which protects animals against hypothermia, obesity, and its associated metabolic disorders (Chouchani et al., 2019; Lowell and Spiegelman, 2000). Previous studies have intensively explored the direct regulation of UCP1's activity, revealing that long-chain fatty acids bind on UCP1 to drive proton leak via a

fatty acid/proton symport mechanism, which dissipates electrochemical energy stored in the proton gradient across the inner mitochondrial membrane. By contrast, purine nucleotides bind on UCP1 to block this uncoupling process, which can be overcome by the elevated concentration of long-chain fatty acids (Bertholet and Kirichok, 2017; Chouchani et al., 2019; Fedorenko et al., 2012). On the other hand, the cysteine oxidation of UCP1, particularly sulfenylation of UCP1 on Cys253, which is triggered by an increase in mitochondrial reactive oxygen species (ROS) elicited by fatty acid oxidation upon adrenergic stimulation, has been shown to be essential for acute cold-induced uncoupled respiration (Chouchani et al., 2016; Shi et al., 2021). Moreover, the lysine succinylation of UCP1 reduces its activity and stability (Wang et al., 2019).

Cytosolic calcium has been shown to directly stimulate adenylyl cyclase activity upon adrenergic stimulation in brown adipocytes, which increases cAMP production and PKA activation to induce lipolysis and thermogenesis (Chen et al., 2017; Maus et al., 2017). As a negative feedback, KCNK3-mediated potassium efflux dampens this adrenergic stimulation-induced calcium influx and its subsequent thermogenic events (Chen et al., 2017). Interestingly, beige adipocytes are equipped with an ATP-dependent and UCP1-independent calcium cycling machinery to dissipate energy as heat, which is composed of two endoplasmic





(A and B) Protein levels (A) and relative mRNA expression (B) of the MCU complex components and UCP1 in the BAT of WT mice housed at 30°C for 4 weeks or 4°C for 1 week.

**Article** 



reticulum-located calcium channels, sarco/endoplasmic reticulum Ca2+-ATPase 2b (SERCA2b) and ryanodine receptor 2 (RyR2) (Ikeda et al., 2017). These studies demonstrate the pivotal roles of intracellular calcium in the regulation of adaptive thermogenesis. The mitochondrion is another important calcium store in the cell. However, whether and how mitochondrial calcium contributes to UCP1-dependent thermogenesis are largely unknown.

As the only identified calcium uniporter and a key regulator of mitochondrial calcium homeostasis, the mitochondrial calcium uniporter (MCU) complex exists as a multi-subunit Ca<sup>2+</sup> channel, consisting of a pore-forming subunit (MCU) and several regulatory subunits including essential MCU regulator (EMRE), mitochondrial calcium uptake 1 (MICU1), MICU2, and MCUb (De Stefani et al., 2016). MCU-mediated mitochondrial Ca<sup>2+</sup> uptake plays an essential role in aerobic metabolism by triggering the tricarboxylic acid (TCA) cycle, electron transfer, and the resultant accumulation of the proton gradient across the inner mitochondrial membrane (i.e., proton motive force) for ATP synthesis (Gherardi et al., 2020). A previous study reported that  $Mcu^{-/-}$ mice exhibited a marked defect upon a peak demand for power output by skeletal muscle (Pan et al., 2013). The activity of MCU varies greatly among tissues, and the direct patch-clamp recording of MCU current density has shown that BAT and skeletal muscle have higher MCU activity compared with other metabolic tissues like the heart, liver, and kidney, suggesting that the MCU may exert physiological functions in BAT (Fieni et al., 2012).

In principle, the MCU-mediated calcium uptake may trigger aerobic respiration to supply protons for uncoupled respiration by UCP1. However, how these two processes are coordinated is unknown. Here, we report that MCU recruits UCP1 through EMRE to form a thermogenic uniporter, named "thermoporter." The adrenergic stimulation-induced thermoporter possesses high calcium channel activity, which enhances calcium influx to accelerate the TCA cycle, NADH production, and proton supply that promotes UCP1-mediated uncoupled respiration. MICU1 acts as a negative regulator of thermogenesis probably through inhibiting thermoporter formation. Accordingly, BAT-specific genetic manipulations of thermopoter assembly, via the deletion of Mcu or Micu1 or expressing linked EMRE-UCP1, markedly regulate thermogenesis and diet-induced obesity and metabolic dysfunction. Our findings uncover a thermoporter that acts as an upstream component of UCP1 operation by controlling its proton flux as a driving force and reveal a physiological role of MCU in BAT.

# **RESULTS**

# **BAT** thermogenesis requires mitochondrial calcium

To investigate the role of MCU in the regulation of uncoupled respiration, we first profiled the expression levels of three MCU complex components in BAT. We found that EMRE was markedly upregulated at both protein and mRNA levels upon cold exposure when compared with thermoneutral acclimation. This upregulation was positively correlated with the increased expression of thermogenic genes like UCP1 and PGC1α (Figures 1A and 1B). To determine the requirement of MCU for BAT thermogenesis, we deleted Mcu specifically in brown adipocytes by crossing Mcufff with Ucp1<sup>Cre</sup> mice (hereafter referred to as McuffUcp1Cre) (Figure S1A). EMRE is required for the uniporter activity and mediates the interaction between MCU and MICU1 in mammalian cells (Sancak et al., 2013). We thus knocked out Emre in brown adipocytes through the local injection of AAV-gRNA into BAT of Rosa26-LSL-Cas9;Adipoq<sup>Cre</sup> mice (Emre-BKO) (Figure S1B). We observed that the absence of MCU did not affect BAT UCP1 content or BAT tissue weight, suggesting that MCU does not regulate BAT development (Figures S1C and S1D). We next examined the cold tolerance of McuffUcp1Cre and Emre-BKO mice by monitoring their core body temperatures under the fasting-cold condition (Schreiber et al., 2017; Shin et al., 2017). Compared with Mcufff controls, McuffUcp1<sup>Cre</sup> mice became hypothermic after a 6-h fastingcold challenge (Figures 1C and S1E-S1G), and similarly, Emre-BKO mice could not maintain their core body temperatures during the challenge (Figures 1D and S1H-S1J). After a 3-week thermoneutral acclimation to 30°C, the core body temperatures of Mcuff Ucp1<sup>Cre</sup> mice were lower than those of Mcuff controls upon acute cold exposure to 4°C (Figure S1K). Infrared thermography analysis showed that the surface temperatures on the interscapular BAT regions of Mcuff Ucp1 Cre and Emre-BKO mice were quantifiably lower than those of respective controls upon the fasting-cold challenge (Figures 1F and 1G). This is consistent with the lower BAT temperatures of McuffUcp1<sup>Cre</sup> mice as measured by implanted temperature probes (Figure 1E).

To address whether the cold intolerance of  $\mathit{Mcu}^{\mathit{fff}}\mathit{Ucp1}^{\mathit{Cre}}$  and Emre-BKO mice was due to impaired BAT thermogenesis rather than shivering thermogenesis of skeletal muscle, we exclusively examined the thermogenic capacity of BAT in McufffUcp1<sup>Cre</sup> and Emre-BKO mice, which was represented by oxygen consumption (VO<sub>2</sub>) induced by the local injection of norepinephrine (NE) into the BAT of anesthetized mice. We found that the NE-induced increase in oxygen consumption was largely blunted in Mcuff fUcp1<sup>Cre</sup> and Emre-BKO mice compared with the respective controls (Figures 1H and 1J). When anesthetized, NE-induced thermogenesis is fueled by fatty acid oxidation in BAT mitochondria (Cannon and Nedergaard, 2004), and consistently, we found that McuffGUcp1Cre and Emre-BKO mice had decreased fat oxidation after NE administration (Figures 1I and 1K). In addition, Mcuf/fUcp1<sup>Cre</sup> mice exhibited similar thermogenic defects as NE stimulation when treated with CL-316,243, a β3-adrenoceptorspecific agonist (Figures S1L and S1M). Together, these results

<sup>(</sup>C and D) Mcu<sup>fff</sup> and Mcu<sup>fff</sup> Local C and Emre-BKO and control mice (D). Core body temperatures during the fasting-cold challenge (n = 6 in C and n = 5 in

<sup>(</sup>E) BAT temperatures of  $Mcu^{flf}$  and  $Mcu^{flf}Ucp1^{Cre}$  mice during the fasting-cold challenge (n = 6 per genotype).

<sup>(</sup>F and G) Mcu<sup>fff</sup> and Mcu<sup>fff</sup> Ucp1<sup>Cre</sup> mice (F) and Emre-BKO and control mice (G). Infrared thermography after 6-h fasting-cold challenge (n = 6 in F and n = 5 in G). (H-K) NE-induced VO<sub>2</sub> (H and J) and fat oxidation (I and K) of anesthetized mice at 32°C (n = 5 per group).

<sup>(</sup>L and M) Mcufff and Mcufff Ucp1<sup>Cre</sup> mice (L) and Emre-BKO and control mice (M). OCR of BAT mitochondria (n = 6 in L and n = 5 in M).

Data are presented as mean ± SEM. \*p < 0.05, \*\*p < 0.01, \*\*\*p < 0.001, and \*\*\*\*p < 0.0001. Two-tailed Student's t test (A, B, F, G, L, and M) or two-way ANOVA followed by Bonferroni post-tests (C-E and H-K). See also Figure S1.



# Cell Metabolism Article

demonstrate that MCU or EMRE deficiency in brown adipocytes specifically impairs non-shivering adaptive thermogenesis.

The impaired thermogenic metabolism of  $Mcu^{f/f}Ucp1^{Cre}$  mice was also reflected in the hematoxylin and eosin staining of the BAT after the fasting-cold challenge: Mcuff BAT exhausted nearly all lipid droplets stored in brown adipocytes, whereas Mcuff/Ucp1<sup>Cre</sup> BAT remained with many unutilized ones due to decreased fatty acid oxidation (Figure S1N). To further explore how the absence of calcium uniporter influences thermogenic metabolism, we examined the uncoupled respiration of BAT mitochondria through the experimental inhibition of UCP1 by guanosine diphosphate (GDP) (Heaton and Nicholls, 1977). Interestingly, we found that the elimination of mitochondrial calcium uptake decreased UCP1-dependent respiration both in McuffUcp1Cre BAT and Emre-BKO BAT, which was rescued by EMRE expression in Emre-BKO BAT (Figures 1L, 1M, and \$10). Collectively, these data demonstrate that MCU is required for UCP1-mediated BAT thermogenesis.

# MCU-EMRE and UCP1 form a complex in brown adipocytes

To determine how MCU regulates uncoupled respiration, we purified the MCU complex from wild-type (WT) BAT overexpressing Strep-tagged MCU followed by mass spectrometry (MS) and found that UCP1 associated with the MCU complex (Figure 2A; Table S1). Through ex vivo co-immunoprecipitation (coIP) experiments, we verified the MCU interaction with UCP1 but not ANT1, another member of the SLC25a family that UCP1 belongs to (Taylor, 2017) (Figure 2B). In addition, blue native PAGE analysis after FLAG-Strep tandem affinity purification showed that MCU-EMRE migrated in 480-650 kDa complexes, and UCP1 co-migrated with MCU complex in the upper fraction at 550-650 kDa. However, the MCU complex migrated faster at 480-550 kDa in the blue native gel when UCP1 was deleted, indicating that UCP1 was incorporated into the native MCU complex in BAT mitochondria (Figure 2C). Besides, immunogold labeling showed that both MCU and UCP1 located on the cristae membrane of BAT mitochondria (Figures S2A and S2B). The knockout of Emre but not Micu1 abrogated MCU association with UCP1, indicating that UCP1 binds MCU in a genetically EMRE-dependent manner (Figures 2D and 2E). To examine whether UCP1 directly binds EMRE, we first generated an Mcu/Emre double knockout HEK 293T cell line (Figure S2C) and then put back MCU and/or EMRE to examine their interactions with UCP1. UCP1 could not pull down the MCU in the absence of EMRE, whereas it interacted with EMRE in the absence of MCU (lines 4 and 5) (Figure 2F). UCP1 could associate with the MCU only in the presence of WT EMRE but not the EMRE (S85W) mutant, which could not interact with the MCU (lines 7 and 8) (Figure 2F) (Tsai et al., 2016), further indicating that EMRE mediates the UCP1-MCU interaction. In addition, UCP1 could not bind MICU1 (line 6) (Figure 2F). To identify specific residues on EMRE or UCP1 for the interaction, we first examined the role of EMRE's only transmembrane helix (TMH) in EMRE-UCP1 interaction. We replaced the TMH with an artificial transmembrane "WALP" helix (GWWLALALALALALAWWA), which does not alter EMRE's mitochondrial location (Killian et al., 1996; Tsai et al., 2016). The EMRE's TMH was reported to be required for the interaction of EMRE-MCU and hence supports calcium permeation. Interestingly, this TMH is also required for the EMRE-UCP1 interaction (Figure 2G). EMRE's G81 and S85 are crucial for EMRE-MCU complex formation (Tsai et al., 2016), we thus asked whether their opposite residues I75 and L83 were responsible for EMRE-UCP1 interaction. We mutated these two residues to tryptophan (W), which might disrupt the helical packing of EMRE and hence its interaction with UCP1, just like EMRE S85W lost its binding capacity with MCU. However, the results showed no difference among EMRE-WT, I75W, and L83W mutants (Figure S2D). We next performed tryptophan scanning mutagenesis to cover all the amino acids with a small side chain (I75 to A90) but failed to identify a single amino acid whose mutation could disrupt EMRE-UCP1 interaction (Figure S2E). We speculate that we might have to mutate several amino acids simultaneously for the disruption of the interaction. Another possibility is that cardiolipin in the inner mitochondrial membrane may contribute to EMRE-UCP1 interaction as in silico and structural analysis showed that both EMRE and UCP1 bind cardiolipin (Jing et al., 2018; Zhuo et al., 2021).

# Adrenergic stimulation induces the assembly of the MCU-EMRE-UCP1 complex

Cold exposure significantly increased MCU-UCP1 interaction and decreased MCU-MICU1 interaction (Figures 3A and 3B), suggesting the MCU-UCP1 interaction may contribute to the requirement of MCU in cold-induced BAT thermogenesis (Figures 1C-1G). In addition, the NE or CL-316,243 treatment increased MCU-EMRE-UCP1 complex formation while it decreased the MCU-EMRE-MICU1 interaction, indicating that adrenergic stimulation can tilt the binding of EMRE by UCP1 over MICU1 (Figures 3C and 3D), and the increased EMRE-UCP1 interaction was partially due to increased EMRE expression upon NE/CL-316,343 treatment (Figures S3A-S3C). This point was further corroborated by the blue native PAGE analysis showing that NE/CL-316.243 treatments considerably promoted the MCU-EMRE-UCP1 complex formation (Figure 3E). Consistently, we found that MICU1 gradually decreased while UCP1 gradually increased their association with the EMRE-MCU complex upon NE/CL stimulation (Figures 3E-3G). Combining the BN-PAGE and coIP results, we can tell that most of the MCU are in a complex with UCP1 upon adrenergic stimulation while only a small proportion (0.86%) of UCP1 associates with MCU (Figures 2C, 3E, 3H, 3I, and S3D). This is rational as a remarkable feature of UCP1 is its abundance in brown adipocytes where it comprises ~8% of the inner mitochondrial membrane proteins (Heaton et al., 1978). Besides, the mRNA expression of UCP1 is 385- or 16-fold higher than MCU and EMRE in brown adipose tissue (Figure 3J) (Meng et al., 2020). Taken together, these findings reveal that adrenergic activation including cold exposure and NE/CL-316,243 treatments can increase MCU-EMRE-UCP1 complex assembly. This point was further supported by impaired MCU-EMRE-UCP1 formation during enhanced MCU-EMRE-MICU1 interaction in ob/ob BAT, which has been recently demonstrated to possess reduced sympathetic innervation compared with WT BAT (Wang et al., 2020) (Figures 3K and 3L).

To investigate how the MCU-EMRE-UCP1 complex formation is regulated by adrenergic stimulation, we first examined whether PKA activation, a common downstream of acute



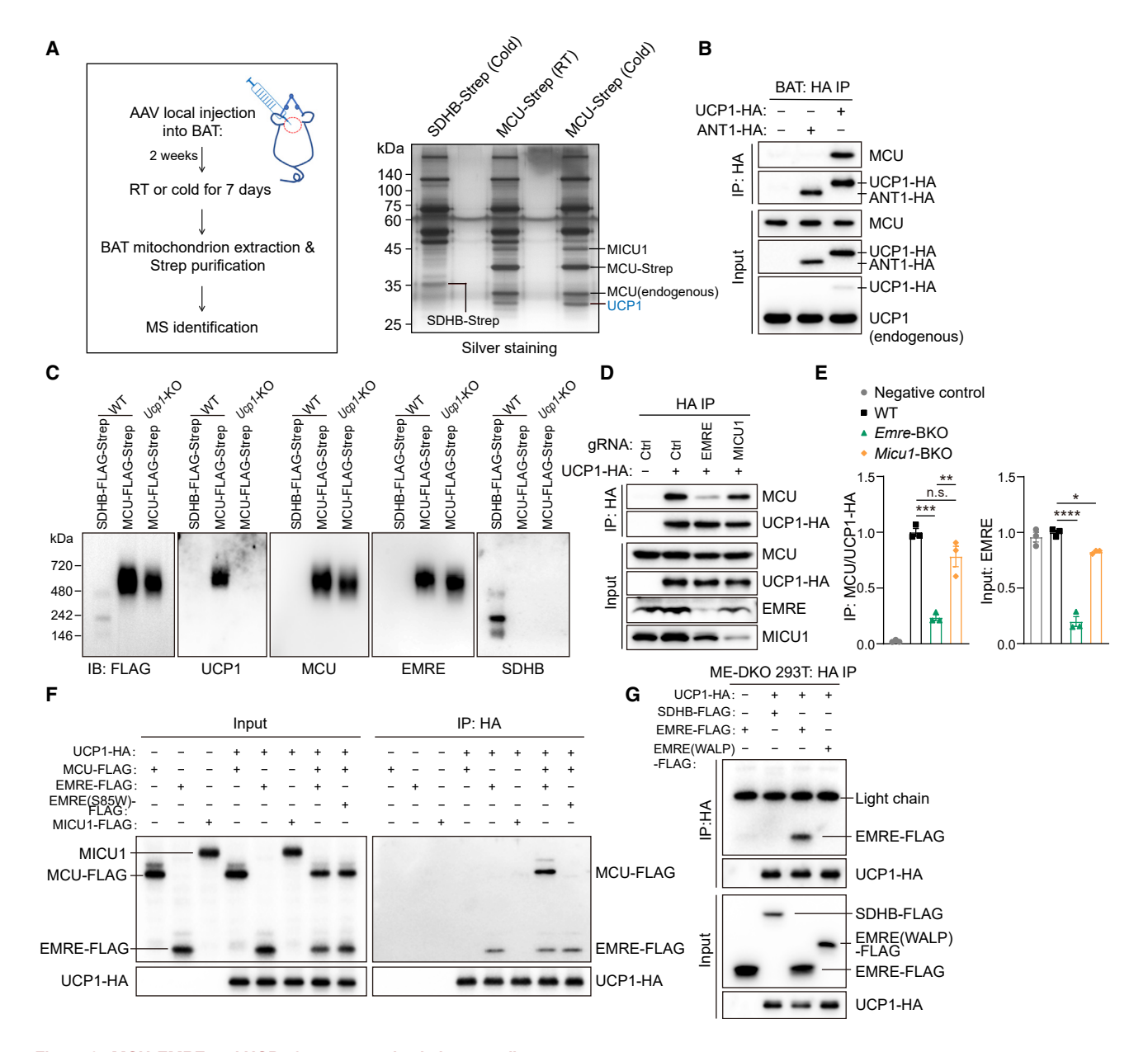


Figure 2. MCU-EMRE and UCP1 form a complex in brown adipocytes

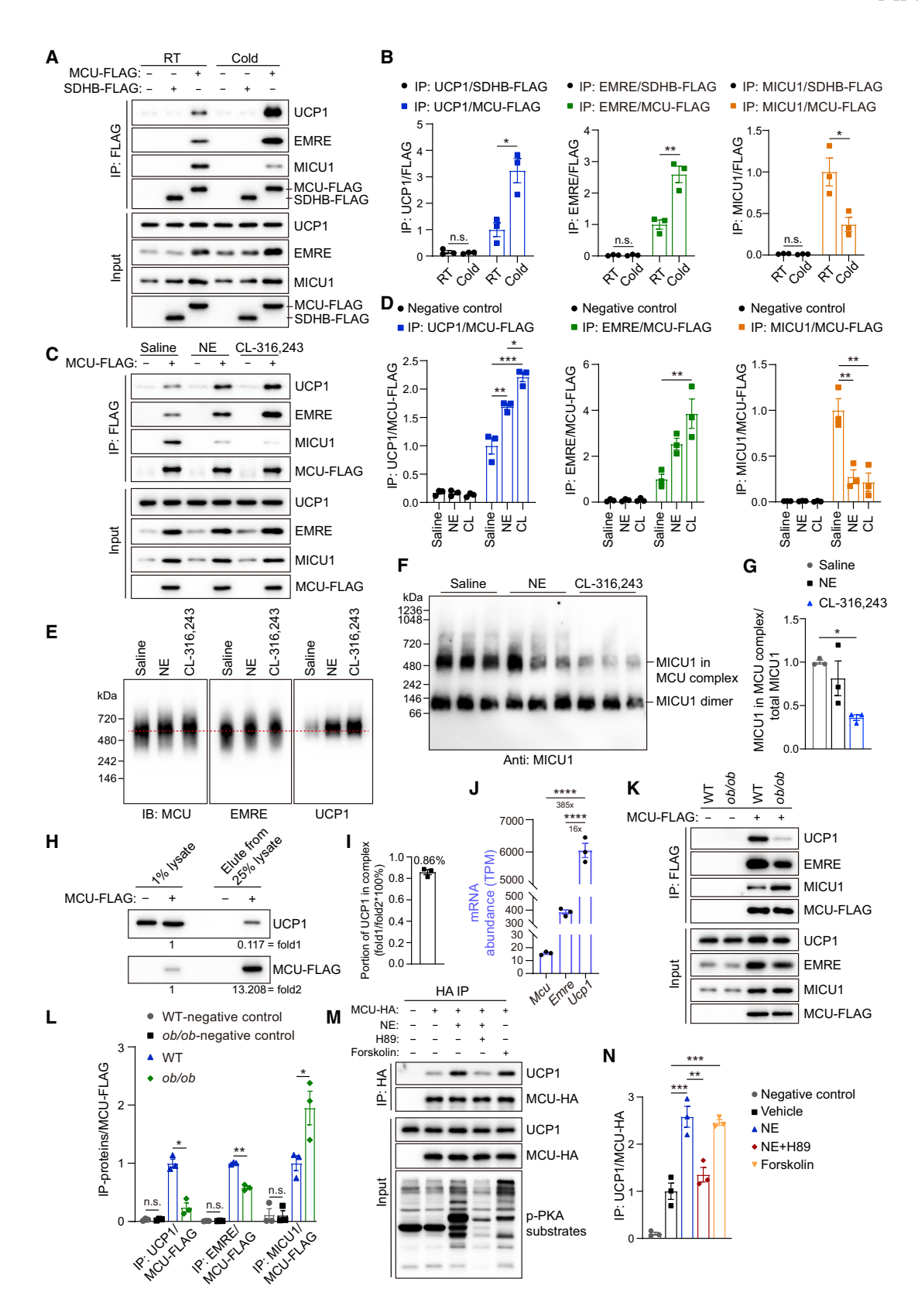
(A) The workflow for MCU complex purification from BAT mitochondria (left). The silver staining of purified MCU-Strep and SDHB-Strep complex from the BAT mitochondria of mice infected with AAV-ADP-MCU-Strep or AAV-ADP-SDHB-Strep (right).

- (B) CoIP analysis of UCP1-HA and endogenous MCU in BAT mitochondria. Non-infected and ANT1-HA controls were included. The expression levels of UCP1-HA and endogenous UCP1 were detected with the UCP1 antibody and shown in the input.
- (C) BN-PAGE analysis of MCU, EMRE, and UCP1 in a large complex purified with MCU-FLAG-Strep from WT and Ucp1-KO BAT mitochondria via FLAG-Strep tandem affinity purification.
- (D) CoIP analysis of UCP1-HA and endogenous MCU using BAT mitochondria from non-infected negative control, WT, Emre-BKO, or Micu1-BKO mice.
- (E) Quantification and statistical analysis of immunoprecipitated endogenous MCU normalized to immunoprecipitated UCP1-HA (left) from experiments as illustrated in (D). The quantification of EMRE expression normalized to MCU (right) as illustrated in the input of (D).
- (F) CoIP experiments showing the interaction between UCP1-HA and FLAG-tagged MCU complex components expressed in ME-DKO 293T cell line.
- (G) CoIP experiments showing the interaction between UCP1-HA and EMRE-FLAG or EMRE(WALP)-FLAG expressed in ME-DKO 293T cell line.

Data are presented as mean ± SEM. \*p < 0.05, \*\*p < 0.01, \*\*\*p < 0.001, and \*\*\*\*p < 0.0001. One-way ANOVA followed by Bonferroni post-tests (E). See also Figure S2.

adrenergic stimulation like cold exposure, NE, and CL treatments, is required and sufficient for the complex formation. Forskolin-induced PKA activation promoted MCU-UCP1 interaction to a similar extent as what the 6-h NE treatment did, whereas the NE-induced interaction was significantly impaired once NE-induced PKA activation was blocked by the H89 compound





# Article



(Figures 3M and 3N). We next determined whether PKA activation-elicited lipolysis plays a role in the complex formation. Unexpectedly, lipolysis blockade did not affect the MCU-UCP1 interaction, indicating others downstream of PKA signaling are responsible for the induced interaction (Figures S3E and S3F). Since all the used adrenergic stimuli increase mitochondrial ROS, which support UCP1-operated respiration through modification of protein thiols, we thus investigate whether ROS regulate this complex formation. However, diamide (a thiol oxidant) did not alter MCU-UCP1 interaction, and the NE-induced interaction was not affected by an inhibition of NE-induced and ROS-mediated modifications of protein thiols by NAC (an antioxidant/thiol reducing agent) (Figures S3G and S3H). These findings indicate that PKA activation is sufficient to induce an acute assembly of the thermoporter and is required for adrenergic stimulation-induced complex formation, independent of lipolysis and ROS-mediated modifications.

# MCU-EMRE-UCP1 complex functions as a "thermoporter"

To reveal how the MCU-EMRE-UCP1 complex regulates BAT thermogenesis, we first examined whether calcium uniporter function is required for the complex formation. We performed ex vivo coIP experiments in McuffUcp1Cre BAT rescued with WT MCU or E263Q mutant (unable to conduct Ca<sup>2+</sup>) (Nguyen et al., 2018) and found that they could interact with UCP1 at a similar level (Figure 4A). However, the obstruction of mitochondrial calcium uptake decreased UCP1-dependent respiration, similar to what we observed in  $Mcu^{f/f}Ucp1^{Cre}$  BAT and Emre-BKO BAT (Figures 1L, 1M, 4B, and 4C), further supporting that mitochondrial calcium uptake is required for BAT thermogenesis. We next asked whether the inducible interaction between MCU-EMRE and UCP1 affects calcium uptake. NE can induce mitochondrial calcium uptake in brown adipocytes from WT but not McuffUcp1Cre BAT or Emre-BKO mice (Figures S4A and S4B), indicating that NE-induced mitochondrial calcium uptake is mediated by MCU. The basal and NE/ isoproterenol (iso)-induced mitochondrial calcium uptake of mature brown adipocytes were increased in the BAT of mice post chronic adrenergic stimulation including cold exposure and NE/CL-316,243 administrations (Figures 4D, 4G, and S4C), accompanied by a faster decline of cytosolic Ca2+ (Figures 4E, 4F, 4H, and 4I). The higher iso-induced mitochondrial calcium uptake in chronic NE/CL-316,243-administrated BAT was not due to their potential effects on mitochondrial structure and function because the expression of related protein and mRNA had almost no change including MCU, MICU1, respiratory complexes components, TCA cycle enzymes, and other membrane transporters (Figures S3A-S3C). CL-316,243 administration promoted the highest MCU activity and fastest buffering rate for cytosolic Ca<sup>2+</sup>, which is congruent with the strongest MCU-UCP1 interaction induced by CL-316,243 (Figures 3C-3E). PDH is a rate-limiting enzyme for the TCA cycle by converting pyruvate into acetyl-CoA and thus controls mitochondrial NADH production. Calcium-sensitive PDP1 (pyruvate dehydrogenase phosphatase 1) dephosphorylates the PDHE1α subunit at S293 to increase PDH enzymatic activity (Karpova et al., 2003). The enhanced mitochondrial calcium uptake upon cold exposure significantly promoted the dephosphorylation of PDHE1α at S293, further supporting that MCU-mediated calcium uptake is involved in the mitochondrial thermogenic metabolism (Figures S4D-S4F).

To investigate whether the formation of the MCU-EMRE-UCP1 complex promotes MCU activity, we constructed an AAV vector that expressed linked EMRE-UCP1 driven by an adiponectin promoter (Figure 4J). The endogenous MCU could interact with overexpressed EMRE-UCP1 in BAT mitochondria as expected but not EMRE(S85W)-UCP1 control since the EMRE(S85W) mutant could not interact with MCU (Tsai et al., 2016) (Figure S4G). Immunofluorescence staining showed a remarkable mitochondrial colocalization of MCU and

# Figure 3. Adrenergic stimulation induces the assembly of the MCU-EMRE-UCP1 complex

- (A) CoIP analysis of MCU-FLAG and endogenous UCP1 using BAT mitochondria from mice housed at RT or post 1-week cold exposure.
- (B) Quantification and statistical analysis of immunoprecipitated UCP1, EMRE, or MICU1 normalized to immunoprecipitated SDHB-FLAG or MCU-FLAG from experiments as illustrated in (A).
- (C) CoIP analysis of MCU-FLAG and endogenous UCP1 using BAT mitochondria from mice with saline, NE, or CL-316,243 administration (7 doses of daily injection, 1 mg/kg body weight).
- (D) Quantification and statistical analysis of immunoprecipitated UCP1, EMRE, or MICU1 normalized to immunoprecipitated MCU-FLAG from experiments as illustrated in (C).
- (E) Blue native PAGE analysis of MCU, EMRE, and UCP1 in MCU complex purified via FLAG-Strep tandem affinity purification from BAT mitochondria of mice injected with AAV-ADP-MCU-FLAG-Strep and administrated with saline, NE, or CL-316,243 (7 doses of daily injection, 1 mg/kg body weight).
- (F) Blue native PAGE analysis of MICU1 in BAT mitochondrial protein lysis from mice administrated with saline, NE, or CL-316,243 (7 doses of daily injection,
- (G) Quantitative and statistical analysis of MICU1 in MCU complex normalized to total MICU1 in (F).
- (H) FLAG-IP analysis of MCU-FLAG and endogenous UCP1 using BAT mitochondria from Mculffucp1<sup>Cre</sup> mice rescued with MCU-FLAG. The mice were challenged with 1-week cold exposure. The experiments were repeated three times.
- (I) Quantification and statistical analysis for a portion of UCP1 interacted with MCU.
- (J) mRNA expression of Mcu, Emre, and Ucp1 in brown adipose tissue, via analyzing their RNA-seq data deposited in a public databank (GEO: GSE90755).
- (K) CoIP analysis of MCU-FLAG and endogenous UCP1 using BAT mitochondria from WT or ob/ob mice.
- (L) Quantification and statistical analysis of immunoprecipitated UCP1, EMRE, or MICU1 normalized to immunoprecipitated MCU-FLAG as illustrated in (K).
- (M) CoIP experiments showing the interaction between MCU-HA and endogenous UCP1 upon NE, "NE+H89," or forskolin treatments in mature brown adipocytes differentiated from BAT SVF. For "NE+H89," brown adipocytes were pretreated with 10 µM H89 for 1 h and then treated with 10 µM NE for another 6 h before harvest. Brown adipocytes were treated with 10  $\mu M$  forskolin for 6 h.
- (N) Quantification and statistical analysis of immunoprecipitated UCP1 normalized to immunoprecipitated MCU-HA as illustrated in (M).
- Data are presented as mean ± SEM. \*p < 0.05, \*\*p < 0.01, \*\*\*p < 0.001, and \*\*\*\*p < 0.0001. Two-tailed Student's t test (B and L) and one-way ANOVA followed by Bonferroni post-tests (D, G, J, and N). See also Figure S3.

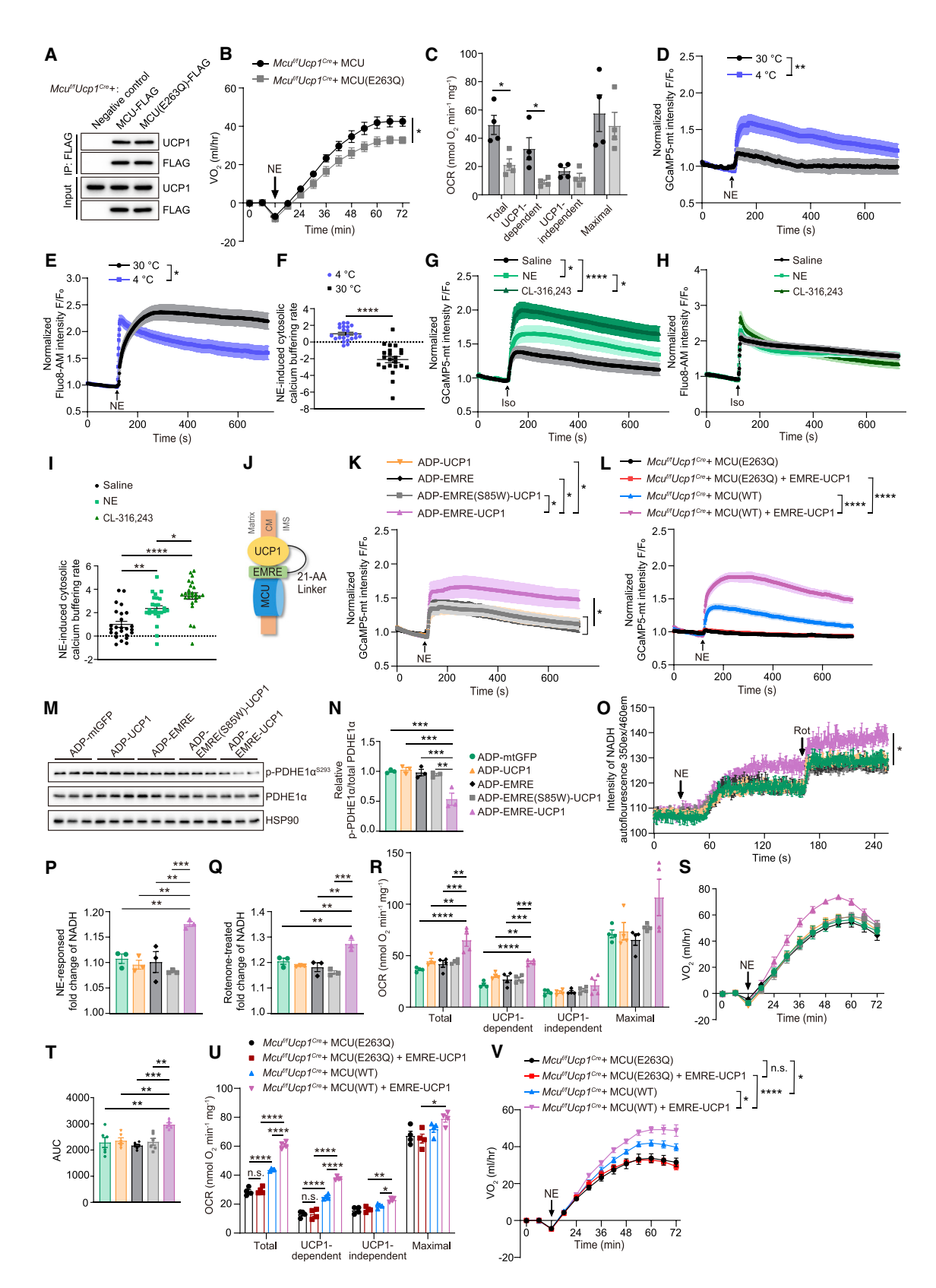


Figure 4. MCU-EMRE-UCP1 complex functions as a "thermoporter" to promote mitochondrial calcium uptake and BAT thermogenesis (A) CoIP analysis of MCU-FLAG, MCU(E263Q)-FLAG and endogenous UCP1 using BAT mitochondria from  $Mcu^{fl}Ucp1^{Cre}$  mice rescued with MCU-FLAG or MCU(E263Q)-FLAG.

Article



EMRE-UCP1 in mature brown adipocytes (Figure S4H). Thus, linked EMRE-UCP1 expression could enforce the MCU-EMRE-UCP1 complex assembly to mimic its increased assembly in BAT mitochondria upon adrenergic stimulation. Strikingly, overexpressed EMRE-UCP1 increased NE-induced mitochondrial Ca<sup>2+</sup> uptake, yet EMRE(S85W)-UCP1, UCP1 alone, or EMRE alone did not (Figures 4K, S4I, and S4J), demonstrating that a specific interaction with UCP1 promotes MCU-mediated mitochondrial calcium influx. When reconstituted the MCU complex in Mcu-BKO BAT with WT MCU or MCU (E263Q) mutant with linked EMRE-UCP1, there was an increased NE-induced mitochondrial calcium uptake in the WT but not E263Q mutant MCU reconstitution (Figures 4L and S4K). This result indicates the linked EMRE-UCP1 promotes mitochondrial Ca<sup>2+</sup> uptake in an MCU-dependent manner. Furthermore, the enhanced MCU activity by interacting with linked EMRE-UCP1 promoted the dephosphorylation of PDHE1 $\alpha$  at S293 (Figures 4M and 4N). Upon NE stimulation, the primary mature brown adipocytes isolated from BAT overexpressing linked EMRE-UCP1 had higher NADH production, thus higher UCP1-mediated uncoupled respiration and NE-induced oxygen consumption (Figures 40-4T). Besides, linked EMRE-UCP1 protein promoted BAT mitochondrial oxygen consumption and thermogenesis in an MCUdependent manner (Figures 4U and 4V). Furthermore, MCU overexpression in BAT increased EMRE protein expression and consequently augment MCU-EMRE-UCP1 interaction (Figures S5A-S5C), accompanied by increased NE-induced mitochondrial Ca2+ uptake, NADH production, oxygen consumption rate (OCR) and hence enhanced mouse thermogenesis, and tolerance to cold exposure (Figures S5D-S5I). These results demonstrate that the induced interaction between MCU-EMRE and UCP1 can enhance MCU activity, which in turn increases UCP1-mediated BAT thermogenesis. Thus, we name the MCU-EMRE-UCP1 complex as "thermoporter," short for thermogenic uniporter, which promotes mitochondrial calcium uptake to enhance BAT thermogenic respiration upon adrenergic stimulation like cold exposure.

# MICU1 negatively regulates thermogenesis probably through inhibiting thermoporter formation and function

MCU activity is tightly regulated by the gatekeeper MICU1 to prevent Ca2+ overload in mitochondria, avoiding bioenergetic crisis and cell death (Csordás et al., 2013; Fan et al., 2020; Mallilankaraman et al., 2012). The physiological regulation of MCU by MICU1 has been intensively studied in the heart and muscles (Gherardi et al., 2020), yet it is unknown whether MICU1 regulates thermogenesis in BAT. MCU-MICU1 interaction markedly decreased upon cold exposure or NE/CL-316,243 treatment (Figures 3A-3D, 3F, and 3G). This was accompanied by an increase in calcium uptake by MCU (Figures 4D and 4G). Micu1 knockout in brown adipocytes through the local injection of AAV-gRNA into Rosa26-LSL-Cas9;Adipoq<sup>Cre</sup> BAT (Micu1-BKO) led to increased basal mitochondrial calcium level (Figure S6A), NE-induced mitochondrial calcium uptake, and cytosolic calcium buffering rate (Figures 5A and 5B). These results indicated that MICU1 functions as a gatekeeper of the MCU complex in BAT just like in other tissues. The increased mitochondrial calcium uptake upon NE stimulation in Micu1-BKO brown adipocytes promoted the dephosphorylation of PDHE1a at S293 and NADH production and thereby enhanced the UCP1-mediated uncoupled respiration and energy expenditure of animals (Figures 5C-5H).

To further characterize the molecular detail underlying the reciprocal regulation between EMRE-MICU1 and EMRE-UCP1 interaction by adrenergic signals (Figures 3A-3G), we disrupted the EMRE-MICU1 interaction by mutating EMRE's carboxyl terminus from the enrichment of aspartic acid (D) to neutral alanine (A) or basic arginine (R) (EMRE-CDA or EMRE-CDR) that mimics the dissociation of MICU1 from MCU-EMRE upon adrenergic stimulation (Tsai et al., 2016). Interestingly, the disruption of EMRE-MICU1 interaction enhanced EMRE-UCP1 association, accompanied by an increased NE-induced mitochondrial calcium uptake, decreased phosphorylation of PDHE1α at S293, and increased NE-induced NADH production and thus enhanced UCP1-mediated uncoupled respiration and BAT

<sup>(</sup>B) NE-induced VO<sub>2</sub> of  $Mcu^{f/f}Ucp1^{Cre}$  mice rescued with MCU(WT) and MCU(E263Q) (n = 6 per group).

<sup>(</sup>C) OCR of BAT mitochondria isolated from  $Mcu''' Ucp1^{Cre}$  mice rescued with MCU(WT) and MCU(E263Q) (n = 4 per group).

<sup>(</sup>D and E) Mitochondrial (D) and cytosolic (E) Ca<sup>2+</sup> kinetics in primary mature brown adipocytes monitored using GCaMP5-mt or Fluo8-AM upon NE (1.5 μM) stimulation. Primary mature brown adipocytes were isolated from mice housed at 30°C for 4 weeks or 4°C for 1 week (n = 25 cells per group in D and n = 22 cells per

<sup>(</sup>F) Relative buffering rates of NE-induced cytosolic Ca<sup>2+</sup> during the first 3 min post NE treatment in (E).

<sup>(</sup>G and H) Mitochondrial (G) and cytosolic (H) Ca<sup>2+</sup> kinetics in primary mature brown adipocytes monitored using GCaMP5-mt or Fluo8-AM upon 1.5 μM iso stimulation. Primary mature brown adipocytes were isolated from mice administrated with NE, CL-316,243, or saline for 7 doses of daily injection (n = 25 cells

<sup>(</sup>I) Relative NE-induced cytosolic Ca<sup>2+</sup> buffering rates during the first 3 min post iso treatment in (H).

<sup>(</sup>J) Model for the linked EMRE-UCP1.

<sup>(</sup>K) Mitochondrial Ca<sup>2+</sup> kinetics in the primary mature brown adipocytes monitored using GCaMP5-mt upon NE (1.5 μM) stimulation. Primary mature brown adipocytes were isolated from mice injected with AAVs expressing EMRE-UCP1, EMRE(S85W)-UCP1, UCP1, or EMRE in BAT (n = 25 cells per group).

<sup>(</sup>L) Mitochondrial Ca<sup>2+</sup> kinetics in primary mature brown adipocytes monitored using GCaMP5-mt upon NE (1.5 μM) stimulation. Primary mature brown adipocytes were isolated from  $Mcu^{f/f}Ucp1^{Cre}$  mice rescued with MCU(WT) or MCU(E263Q), plus EMRE-UCP1 or not (n = 30 cells per group).

<sup>(</sup>M and N) PDH phosphorylation at S293 of the E1α subunit and total PDH expression in the BAT of mice upon 1-h cold exposure.

<sup>(</sup>O-Q) NADH autofluorescence in mature brown adipocytes upon treatment with NE (10 µM) followed by the addition of rotenone (2 µM) (O). NE-responded (P) and rotenone-treated (Q) fold change of NADH relative to basal NADH level.

<sup>(</sup>R) OCR of BAT mitochondria isolated from mice injected with AAVs (n = 4 per group).

<sup>(</sup>S and T) NE-induced VO<sub>2</sub> (S) and area under the curve (AUC) (T) of mice injected with AAVs (n = 6 per group).

<sup>(</sup>U) OCR of BAT mitochondria isolated from  $Mcu^{ff}Ucp1^{Cre}$  mice rescued with MCU(WT) or MCU(E263Q), plus EMRE-UCP1 or not (n = 4 per group).

<sup>(</sup>V) NE-induced VO<sub>2</sub> of anesthetized mice at 32°C (n = 5 per group).

Data are presented as mean ± SEM. \*p < 0.05, \*\*p < 0.01, \*\*\*p < 0.001, and \*\*\*\*p < 0.0001. Two-tailed Student's t test (C and F), two-way ANOVA followed by Bonferroni post-tests (B, D, E, G, K, L, O, and V), or one-way ANOVA followed by Bonferroni post-tests (I, N, P-R, and T). See also Figures S4 and S5.



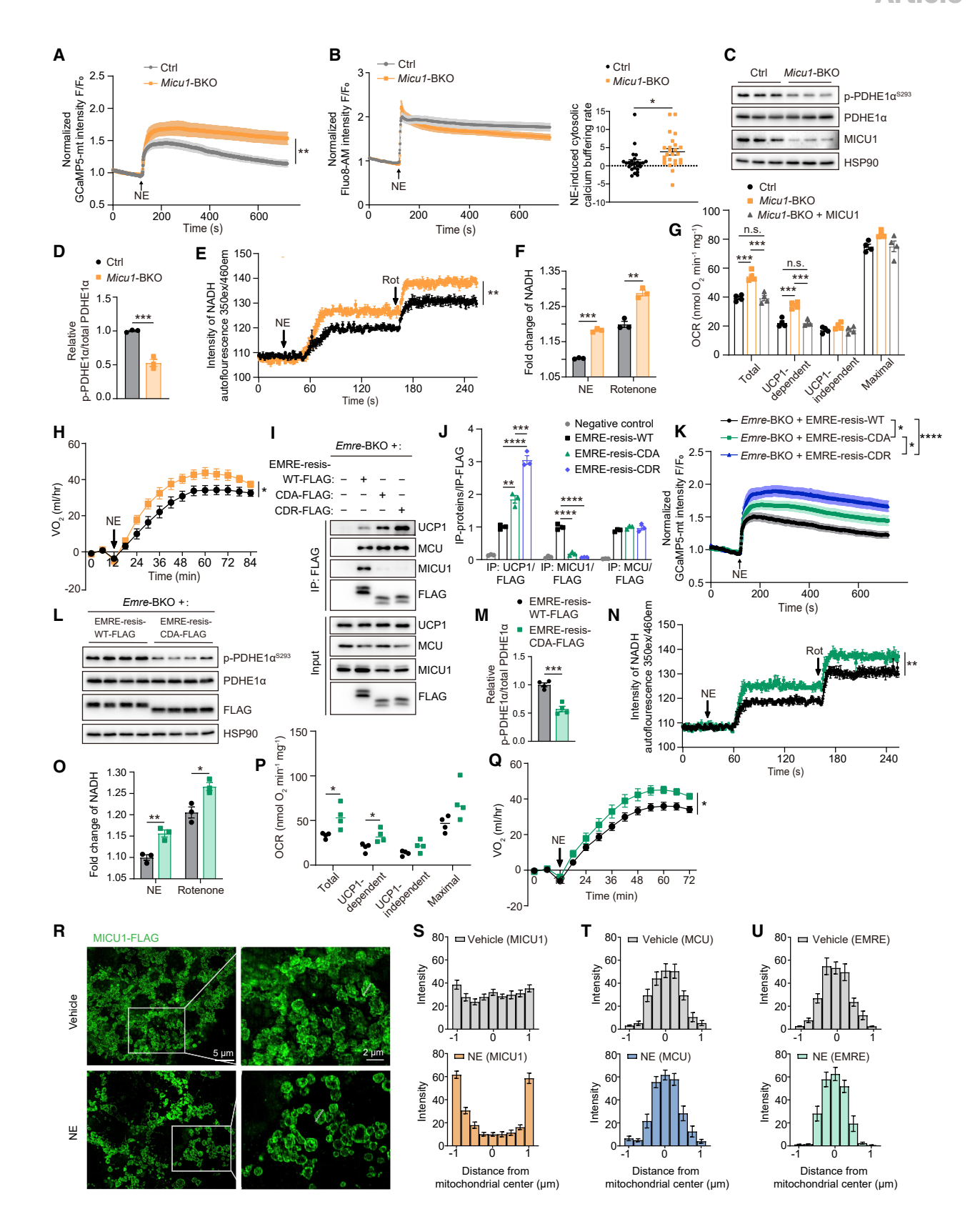


Figure 5. MICU1 negatively regulates thermogenesis probably through inhibiting thermoporter formation and function
(A) Mitochondrial Ca<sup>2+</sup> kinetics in primary mature brown adipocytes monitored using GCaMP5-mt upon NE (1.5 μM) stimulation. Primary mature brown adipocytes were isolated from Ctrl and *Micu1*-BKO mice (n = 25 cells per group).

# **Article**



thermogenic capacity (Figures 5I-5Q). These results suggest a negative regulatory role of MICU1 in the MCU-EMRE-UCP1 interaction (i.e., thermoporter formation), probably through a steric hindrance effect. In support of this point, immunofluorescence staining in mature brown adipocytes showed that NE treatment promoted the translocation of MICU1 from the mitochondria cristae membrane to the inner boundary membrane (Figures 5R and 5S). However, the MCU and EMRE maintained on the mitochondria cristae membrane upon NE stimulation (Figures 5T, 5U, S6B, and S6C). Taken together, these findings reveal that MICU1 in BAT acts as a negative regulator for thermogenesis through the gatekeeping of mitochondrial calcium uptake and probably inhibiting thermoporter formation (Figure S6D).

# Thermoporter assembly serves as a target against obesity

Having established that such an adrenergic-inducible thermoporter assembly could promote BAT thermogenesis (Figures 4R and 4S), we next investigated whether targeting thermoporter assembly could correct thermogenic defects to protect against obesity and its associated metabolic dysfunction. First, we examined whether the enforced assembly of this thermoporter by expressing linked EMRE-UCP1 could alleviate cold intolerance of ob/ob mice, which have defective thermogenesis resulting from reduced sympathetic innervation of BAT and scWAT (Wang et al., 2020). Indeed, the enforced assembly of the thermoporter in ob/ob BAT endowed mice with higher core body temperature than controls during acute cold exposure, attributing to enhanced thermogenic capacity regardless of less sympathetic innervation (Figures 6A, 6B, and S7A). Second, we expressed linked EMRE-UCP1 in mouse BAT and then fed a high-fat diet (HFD). We observed that mice carrying enforcedly assembled thermoporter gained less body weight, particularly fat mass, getting more tolerant to glucose and insulin, respectively, and more sensitive to insulin stimulation in the fat, liver, and muscle, along with increased animal energy expenditure (Figures 6C-6J and S7B-S7D). Third, we knocked out Micu1 in brown adipocytes to increase thermoporter assembly and activity and fed HFD. We observed similar phenotypes as those of expressing linked EMRE-UCP1 upon HFD feeding, including less weight gain, particularly fat mass, improved glucose homeostasis, and systemic insulin sensitivity, again with increased animal energy metabolism (Figures 7A-7F and S7E-S7J). Last, we deleted Mcu in brown adipocytes to eliminate thermoporter and then fed HFD. As expected, we observed opposite metabolic phenotypes such as more weight gain, particularly fat mass, exacerbated glucose homeostasis, and impaired systemic insulin sensitivity, due to reduced animal energy expenditure and BAT mitochondrial metabolism (Figures 7G-7L and S7K-S7N). Collectively, these findings support that targeting thermoporter assembly is a promising therapeutic strategy against obesity and its associated metabolic disorders.

#### DISCUSSION

Since the discovery of brown and beige fat in adult humans and their implications for obesity treatment, an explosive number of studies have been carried out to investigate how to increase adipose tissue thermogenesis with UCP1 as a major target (Chouchani et al., 2019; Wang and Seale, 2016). Yet it remains largely unknown how the operation of UCP1-mediated BAT thermogenesis is regulated. Using genetic mouse models including the BAT-specific deletion of Mcu, Emre, Micu1, and BAT-specific expression of linked EMRE-UCP1, we demonstrate that under cold exposure or adrenergic stimulation conditions, the MCU recruits UCP1 through EMRE to form a thermoporter that possesses high calcium channel activity. Enhanced mitochondrial calcium influx accelerates the TCA cycle, NADH production, and proton supply to promote UCP1-mediated uncoupled respiration. MICU1 acts as a negative regulator of thermogenesis probably through inhibiting thermoporter formation (Figure S6D). To our knowledge, this is the first study that directly links two fundamental mitochondrial processes in brown adipose tissue: UCP1-mediated uncoupled respiration and MCU-mediated aerobic respiration. Our findings reveal how these two respiratory

(B) Cytosolic Ca2+ kinetics in primary mature brown adipocytes monitored using Fluo8-AM upon NE (1.5 µM) stimulation (left). Primary mature brown adipocytes were isolated from Ctrl and Micu1-BKO mice (n = 25 cells per group). Relative buffering rates of NE-induced cytosolic Ca2+ during the first 3 min post NE treat-

(C and D) PDH phosphorylation at S293 of the E1α subunit and total PDH expression in BAT of Micu1-BKO and control mice upon 1-h cold exposure.

(E and F) NADH autofluorescence in mature brown adipocytes of Micu1-BKO and control mice (n = 3 per group).

(G) OCR of BAT mitochondria isolated from Ctrl, Micu1-BKO, and MICU1-rescued mice (n = 4 per group).

(H) NE-induced  $VO_2$  of *Micu1*-BKO and control mice (n = 5 per group).

(I) CoIP analysis of EMRE-FLAG and endogenous UCP1 using BAT mitochondria from Emre-BKO mice rescued with EMRE-WT-FLAG, EMRE-CDA-FLAG, or EMRE-CDR-FLAG.

(J) Quantification and statistical analysis of immunoprecipitated UCP1, MCU, or MICU1 normalized to immunoprecipitated EMRE-WT-FLAG, EMRE-CDA-FLAG, and EMRE-CDR-FLAG as illustrated in (I).

(K) Mitochondrial Ca<sup>2+</sup> kinetics in primary mature brown adipocytes monitored using GCaMP5-mt upon NE (1.5 μM) stimulation. Primary mature brown adipocytes were isolated from Emre-BKO mice rescued with EMRE-WT-FLAG, EMRE-CDA-FLAG, or EMRE-CDR-FLAG (n = 26 cells per group).

(L and M) PDH phosphorylation at S293 of the E1α subunit and total PDH expression in BAT of Emre-BKO mice rescued with EMRE-WT or EMRE-CDA.

(N and O) NADH autofluorescence in mature brown adipocytes of Emre-BKO mice rescued with EMRE-WT or EMRE-CDA (n = 3 per group).

(P) OCR of BAT mitochondria isolated from Emre-BKO mice rescued with EMRE-WT or EMRE-CDA in BAT (n = 4 per group).

(Q) NE-induced VO<sub>2</sub> of Emre-BKO mice rescued with EMRE-WT or EMRE-CDA in BAT (n = 5 per group).

(R-U) Immunofluorescence staining analysis of the localization of MICU1-FLAG, MCU-FLAG, and EMRE-FLAG in primary mature brown adipocytes isolated from mice administrated with vehicle or NE for 7 doses of daily injection. The quantification of the spatial-intensity distribution of (R and S) MICU1-FLAG, (T) MCU-FLAG, and (U) EMRE-FLAG relative to the mitochondrial center are shown by white-dotted lines.

Data are presented as mean ± SEM. \*p < 0.05, \*\*p < 0.01, \*\*\*p < 0.001, and \*\*\*\*p < 0.0001. Two-tailed Student's t test (B, D, F, M, O, and P), two-way ANOVA followed by Bonferroni post-tests (A, E, H, K, N, and Q), or one-way ANOVA followed by Bonferroni post-tests (G and J). See also Figure S6.

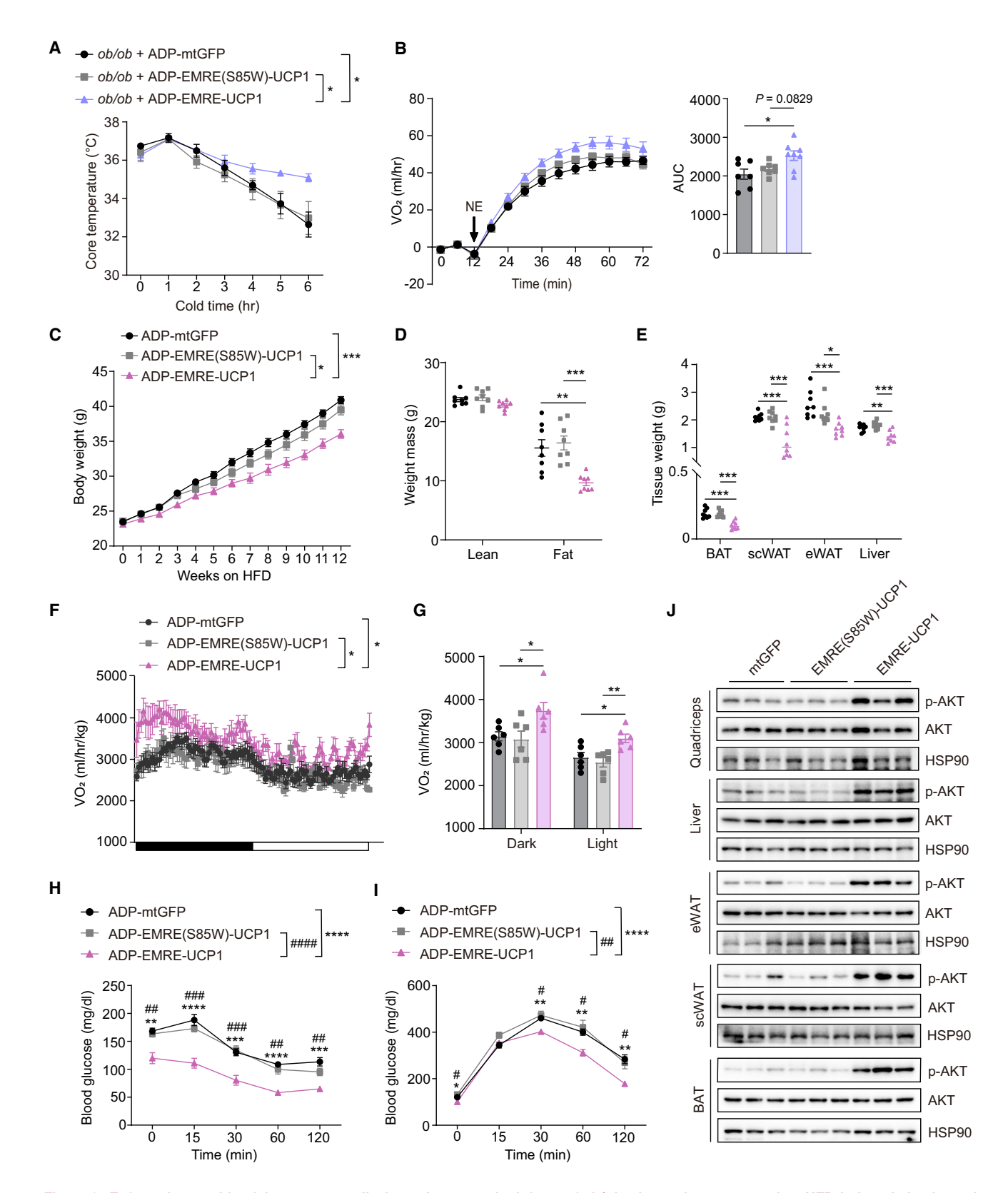


Figure 6. Enforced assembly of thermoporter alleviates thermogenic defects of *ob/ob* mice and protects against HFD-induced obesity and metabolic dysfunction

(A) Core body temperatures of *ob/ob* mice injected with AAVs expressing EMRE-UCP1, EMRE(S85W)-UCP1, and mtGFP in BAT during cold exposure (n = 7 per group).

# Article



machineries physically interact to orchestrate cellular energy expenditure. This model suggests an unexpected role of UCP1 as a signaling molecule in the regulation of adaptive thermogenesis, i.e., acting as an accelerator of calcium uniporter to provide sustainable proton flux as a driving force for UCP1's uncoupling operation. Thus, this novel mechanism adds another regulatory layer for UCP1's uncoupling process besides direct modulations of its own activity (Chouchani et al., 2016; Fedorenko et al., 2012; Shi et al., 2021; Wang et al., 2019).

About 10 years after the molecular identification of the key MCU complex components (MCU and MICU1) (Baughman et al., 2011; De Stefani et al., 2011; Perocchi et al., 2010), many studies have been performed to explore its organismal physiology through the genetic manipulation of Mcu or Micu1, particularly in skeletal and cardiac muscle as Mcu knockout in mice and MICU1 truncation in humans both primarily cause skeletal muscle defects (Gherardi et al., 2020; Lewis-Smith et al., 2016; Logan et al., 2014; Pan et al., 2013). Mcu deletion was lethal for C57BL/6 mice, whereas Mcu<sup>-/-</sup> mice on a CD1 background were viable, though with fewer offspring, suggesting a considerable influence of genetic background on MCU's physiological outputs (Murphy et al., 2014). Surprisingly, the MCU complex seems not essential for maintaining normal physiology in adult mice. Mcu<sup>-/-</sup> mice showed reduced sprinting exercise performance that required a maximal power output by skeletal muscle (Kwong et al., 2018; Pan et al., 2013). On the other hand, constitutive or cardiac-specific loss of uniporter activity by either the deletion of Mcu or the overexpression of dominant-negative Mcu or of Mcub (a negative regulator of the uniporter) was also dispensable for heart function at the basal line. However, they all showed a blunted increase in the heart rate during the "fight-or-flight" response and did not survive the ischemiareperfusion (IR) injury (Gherardi et al., 2020). These findings suggest that strong adrenergic stimulation is a prerequisite for probing the physiological function of the MCU complex. In isolated brown adipocytes, the mobilization of intracellular Ca2+ stores by NE stimulation was observed about 4 decades ago (Connolly et al., 1984). Until recently, the function of this Ca<sup>2+</sup> mobilization in BAT thermogenesis has been systemically investigated, revealing that KCNK3 serves as a negative regulator of thermogenesis by inhibiting Ca<sup>2+</sup> influx-induced cAMP production, lipolysis, and thermogenic respiration (Chen et al., 2017). In our study, we demonstrate the function and mechanism of mitochondrial calcium for promoting UCP1-mediated uncoupled respiration. However, a previous study by Flicker and colleagues reported that Mcu knockout in brown adipocytes had no effects on diet-induced obesity and cold tolerance (Flicker et al., 2019). It is worth noting that their Mcu<sup>f/f</sup>Ucp1<sup>Cre</sup> mice were on mixed genetic backgrounds (~95% C57BL/6J plus ~5% 129) while our mice were on a pure C57BL/ 6J background, which probably accounts for the different dietinduced obesity phenotypes. In our cold tolerance test experiments, the core body temperatures of Mcuff Ucp1 Cre mice were comparable with those of Mcufff mice during the first 6 h when shifted from 30°C to 4°C, similar to what Flicker et al. observed (Figure S1K). However, when mice were cold-challenged for a longer time, the body temperatures of Mcuff Ucp1<sup>Cre</sup> mice became lower than those of Mcufff mice, starting from the 7-h post-cold exposure (Figure S1K). When we challenged mice with a more severe condition, fasting-cold, the thermogenic defect of Mcuf/-<sup>f</sup>Ucp1<sup>Cre</sup> mice was augmented as shown by the earlier and larger reduction of core body temperature (Figure 1C). Like in the skeletal and cardiac muscle, the BAT MCU complex exhibits significant function in response to strong adrenergic stimuli including longtime cold exposure or fasting-cold challenge. In this regard, the thermoporter assembly increases the animals' thermogenic capacity and thus confers a fitness and survival advantage under a hostile environment like long-time cold exposure and fastingcold challenge that warm-blooded wild animals would encounter during the winter.

We have also provided a proof-of-concept for the therapeutic implications of the novel mechanism. Through the loss-of-function knockout of BAT Mcu or Emre to delete the thermoporter, mice became thermogenically defective, obese-prone, and metabolically dysfunctional. By sharp contrast, through gain of function to enhance thermoporter activity either by the deletion of BAT Micu1 or via the enforced assembly of the thermoporter using linked EMRE-UCP1 but not EMRE or UCP1 alone, mice acquired greater thermogenic capacity and became obesity-resistant and metabolically healthy. Noticeably, the enforced assembly of the thermoporter significantly improved the thermogenic defects of ob/ob mice even under the condition of low adrenergic input and UCP1 expression (Wang et al., 2020). Thus, it is tempting to speculate that it will greatly improve the BAT thermogenic capacity of obese patients if one employs a combinatory therapy that simultaneously increases BAT sympathetic innervation and its downstream effector, the thermoporter's assembly and activity.

# **Limitations of study**

The primary goal of this study was to reveal whether and how MCU-mediated mitochondrial calcium signaling regulates uncoupled respiration. We have demonstrated that the MCU-EMRE-UCP1 complex (thermoporter) plays a critical role and extensively explored how UCP1 interacts with EMRE through different physiological, chemical, and genetic manipulation. Although we have demonstrated the requirement of the TMH of EMRE for the EMRE-UCP1 interaction, we have not determined the exact residue(s) responsible for the interaction by the singleamino-acid tryptophan scanning mutagenesis of EMRE's TMH,

(B) NE-induced VO<sub>2</sub> of ob/ob mice injected with AAVs as in (A) and AUC of NE-induced VO<sub>2</sub> (n = 7 for EMRE(S85W)-UCP1 and mtGFP; n = 8 for EMRE-UCP1). (C) Body weight curves of WT mice injected with AAVs expressing EMRE-UCP1, EMRE(S85W)-UCP1, and mtGFP in BAT and fed with HFD (n = 8 per group). (D and E) Fat mass and lean mass (D) and tissue weight (E) of HFD-fed mice in (C) (n = 8 per group). (F and G) VO<sub>2</sub> of HFD-fed mice in (C) (n = 6 per group).

<sup>(</sup>H and I) Insulin tolerance test (H) and glucose tolerance test (I) of mice in (C) (n = 8 per group).

<sup>(</sup>J) Assessment of insulin sensitivity as measured by phosphorylation of AKT in mice of (C).

Data are presented as mean ± SEM. \*p < 0.05, \*\*p < 0.01, \*\*\*p < 0.001, and \*\*\*\*p < 0.0001. Two-way ANOVA followed by Bonferroni post-tests (A, C, F, H, and I) or a one-way ANOVA followed by Bonferroni post-tests (B, D, E, and G). (H and I) Multiple comparisons of data points: ADP-EMRE-UCP1 versus ADP-EMRE (S85W)-UCP1 or ADP-mtGFP. See also Figure S7.

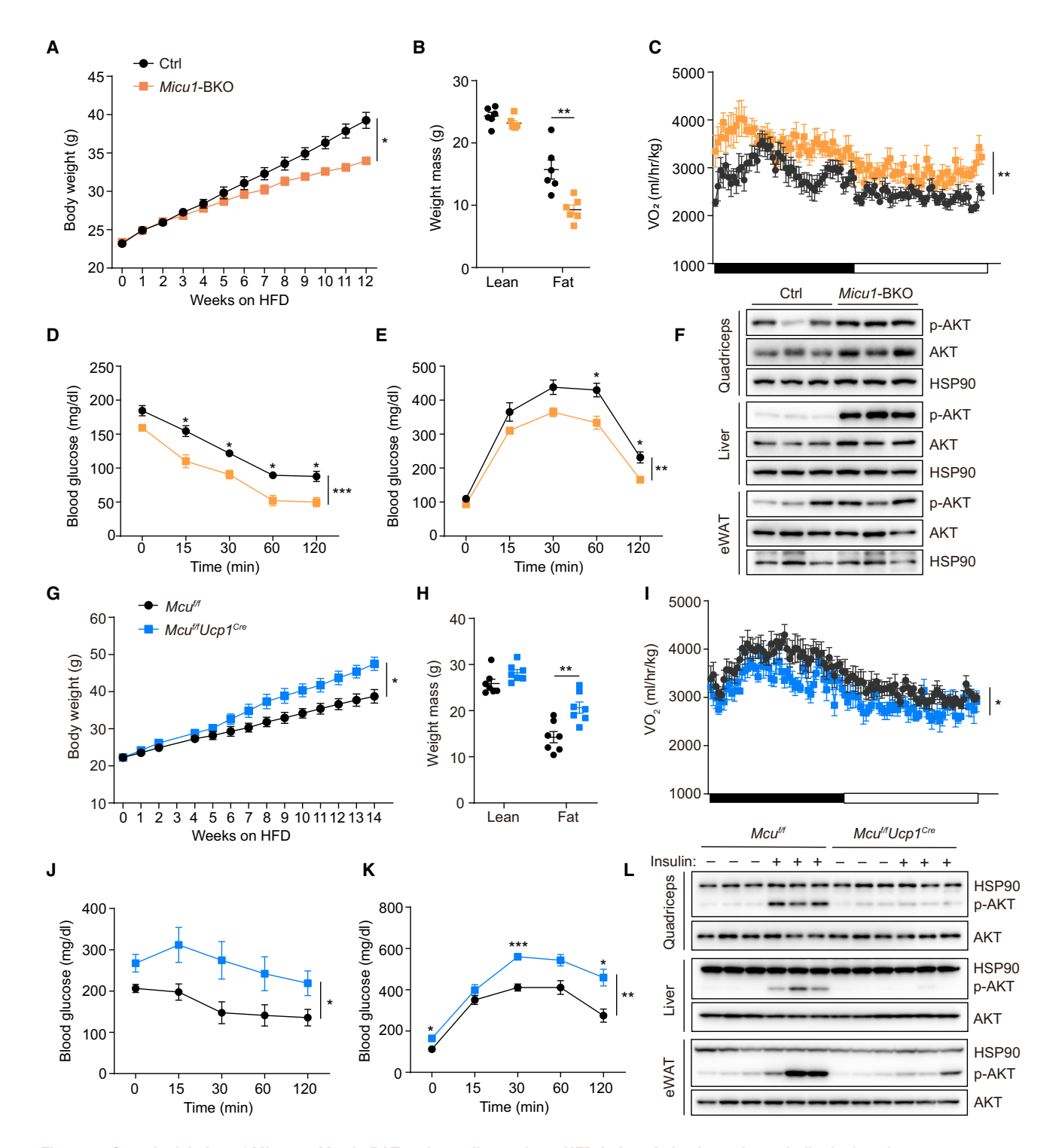


Figure 7. Genetic deletion of *Micu1* or *Mcu* in BAT reciprocally regulates HFD-induced obesity and metabolic dysfunction (A–E) Body weight curves (A), fat mass and lean mass (B), VO<sub>2</sub> (C), insulin tolerance test (D), and glucose tolerance test (E) of *Micu1*-BKO and control mice fed HFD

(F) Assessment of insulin sensitivity as measured by the phosphorylation of AKT in Micu1-BKO and control mice fed HFD.

(G-K) Body weight curves (G), fat mass and lean mass (H), VO<sub>2</sub> (I), insulin tolerance test (J), and glucose tolerance test (K) of Mcu<sup>III</sup> and Mcu<sup>III</sup> Ucp1<sup>Cre</sup> mice fed HFD (n = 7 per group; n = 6 for VO<sub>2</sub>).

(L) Assessment of insulin sensitivity as measured by phosphorylation of AKT in  $Mcu^{f/f}$  and  $Mcu^{f/f}$  ucp1 $^{Cre}$  mice fed HFD.

Data are presented as mean  $\pm$  SEM. \*p < 0.05, \*\*p < 0.01, \*\*\*p < 0.001, and \*\*\*\*p < 0.0001. Two-way ANOVA followed by Bonferroni post-tests (A, C–E, G, and I–K) or two-tailed Student's t test (B and H). See also Figure S7.

# **Article**



suggesting that multiple amino acids of EMRE are involved. Besides, cardiolipin in the inner mitochondrial membrane may contribute to the EMRE-UCP1 interaction. Thus, it warrants further investigation to solve the structure of MCU-EMRE-UCP1 and compare it with that of MCU-EMRE-MICU1, which will facilitate the detailed understanding of the competition between MICU1 and UCP1 for binding EMRE and hence help design precise strategies modulating the assembly and activity of the thermoporter.

# **STAR**\*METHODS

Detailed methods are provided in the online version of this paper and include the following:

- KEY RESOURCES TABLE
- RESOURCE AVAILABILITY
  - Lead contact
  - Materials availability
  - Data and code availability
- EXPERIMENTAL MODEL AND SUBJECT DETAILS
  - Animal models
  - Primary cell culture
- METHOD DETAILS
  - Western blot
  - Gene expression analysis
  - Measurement of core body temperature
  - Measurement of BAT temperature with implanted probe
  - Infrared thermographic imaging
  - O Energy expenditure and body composition measurements
  - Isolation of BAT mitochondria
  - Oxygen consumption
  - O Construct design and site-directed mutagenesis
  - AAV injection into BAT
  - Strep purification followed by mass spectrometry (MS)
  - Co-immunoprecipitation (co-IP)
  - Blue native PAGE
  - Immuno-electronmicroscopy (IEM)
  - O Measurement of NE-induced mitochondrial calcium uptake in primary mature brown adipocytes
  - Immunofluorescence
  - O NADH production in isolated primary mature brown adipocytes
  - O Intraperitoneal insulin tolerance test and glucose tolerance test
  - Insulin sensitivity
  - O Tissue hematoxylin and eosin (H&E) staining
- QUANTIFICATION AND STATISTICAL ANALYSIS

# SUPPLEMENTAL INFORMATION

Supplemental information can be found online at https://doi.org/10.1016/j. cmet.2022.07.011.

# **ACKNOWLEDGMENTS**

We thank the members of the Qiu laboratory, Drs. Yong Liu (Wuhan University), Hansong Ma (University of Cambridge), and Xiaolei Su (Yale University) for their comments on the manuscript. We thank Drs. Ruiping Xiao and Yan Zhang (Peking University) for sharing ob/+ mice, Drs. Heping Cheng and Xianhua Wang (Peking University) for sharing the GCaMP5-mt plasmid and for the use of their spectrofluorophotometer (RF-5301PC), and Drs. Yiguo Wang (Tsinghua University) and Wanzhu Jin (IOZ/CAS) for the use of their telemetric temperature sensor and FLIR T530 infrared camera, respectively. We thank Dr. Xiuqin Zhang at the pathology core facility of the Institute of Molecular Medicine, Peking University for the H&E staining analysis. We thank Drs. Ying-Chun Hu, Si-Ying Qin, Peng-Yuan Dong, and Yun-Chao Xie for their technical assistance with the EM sample preparation and image analysis at the Core Facilities of the School of Life Sciences, Peking University. We also thank Dr. Haiteng Deng and Xianbin Meng in the Proteinomics Facility at the Technology Center for Protein Sciences, Tsinghua University for the protein MS analysis. This work was supported by grants from the National Key R&D Program of China (2018YFA0800702 and 2021YFA0804801), the National Natural Science Foundation of China (31671227 and 91642113), and the Thousand Young Talents Program of the Chinese Government to Y.Q. All the animal care and procedures were performed in accordance with PKU IACUC guidelines.

#### **AUTHOR CONTRIBUTIONS**

K.X. and D.W. designed and performed the main experiments with assistance from Y.W., Y.Z., H.S., J.Y., X.H., X.L., Z.Z., and Z.W.; K.X., D.W., and Y.Q. discussed and interpreted the results from the study; and K.X., D.W., and Y.Q. conceived, supervised, and wrote the paper.

#### **DECLARATION OF INTERESTS**

The authors declare no competing interests.

Received: August 16, 2021 Revised: March 3, 2022 Accepted: July 25, 2022 Published: August 16, 2022

### REFERENCES

Baughman, J.M., Perocchi, F., Girgis, H.S., Plovanich, M., Belcher-Timme, C.A., Sancak, Y., Bao, X.R., Strittmatter, L., Goldberger, O., Bogorad, R.L., et al. (2011). Integrative genomics identifies MCU as an essential component of the mitochondrial calcium uniporter. Nature 476, 341-345.

Bertholet, A.M., and Kirichok, Y. (2017). UCP1: a transporter for H+ and fatty acid anions. Biochimie 134, 28-34.

Bradley, A., Anastassiadis, K., Ayadi, A., Battey, J.F., Bell, C., Birling, M.C., Bottomley, J., Brown, S.D., Bürger, A., Bult, C.J., et al. (2012). The mammalian gene function resource: the International Knockout Mouse Consortium. Mamm. Genome 23, 580-586.

Cannon, B., and Nedergaard, J. (2004). Brown adipose tissue: function and physiological significance. Physiol. Rev. 84, 277–359.

Cao, Y. (2010). Adipose tissue angiogenesis as a therapeutic target for obesity and metabolic diseases. Nat. Rev. Drug Discov. 9, 107-115.

Chen, Y., Zeng, X., Huang, X., Serag, S., Woolf, C.J., and Spiegelman, B.M. (2017). Crosstalk between KCNK3-mediated ion current and adrenergic signaling regulates adipose thermogenesis and obesity. Cell 171, 836-848.e13.

Chouchani, E.T., Kazak, L., Jedrychowski, M.P., Lu, G.Z., Erickson, B.K., Szpyt, J., Pierce, K.A., Laznik-Bogoslavski, D., Vetrivelan, R., Clish, C.B., et al. (2016). Mitochondrial ROS regulate thermogenic energy expenditure and sulfenylation of UCP1. Nature 532, 112-116.

Chouchani, E.T., Kazak, L., and Spiegelman, B.M. (2019). New advances in adaptive thermogenesis: UCP1 and beyond. Cell Metab. 29, 27-37.

Connolly, E., Nånberg, E., and Nedergaard, J. (1984). Na+-dependent, alphaadrenergic mobilization of intracellular (mitochondrial) Ca2+ in brown adipocytes. Eur. J. Biochem. 141, 187-193.

Csordás, G., Golenár, T., Seifert, E.L., Kamer, K.J., Sancak, Y., Perocchi, F., Moffat, C., Weaver, D., Perez, S.F., Bogorad, R., et al. (2013). MICU1 controls both the threshold and cooperative activation of the mitochondrial Ca2+ uniporter. Cell Metab. 17, 976-987.



# **Cell Metabolism**Article

De Stefani, D., Raffaello, A., Teardo, E., Szabò, I., and Rizzuto, R. (2011). A forty-kilodalton protein of the inner membrane is the mitochondrial calcium uniporter. Nature *476*, 336–340.

De Stefani, D., Rizzuto, R., and Pozzan, T. (2016). Enjoy the trip: calcium in mitochondria back and forth. Annu. Rev. Biochem. 85, 161–192.

Dietrich, M.O., and Horvath, T.L. (2012). Limitations in anti-obesity drug development: the critical role of hunger-promoting neurons. Nat. Rev. Drug Discov. *11*, 675–691.

Fan, M., Zhang, J., Tsai, C.W., Orlando, B.J., Rodriguez, M., Xu, Y., Liao, M., Tsai, M.F., and Feng, L. (2020). Structure and mechanism of the mitochondrial Ca<sup>2+</sup> uniporter holocomplex. Nature *582*, 129–133.

Fedorenko, A., Lishko, P.V., and Kirichok, Y. (2012). Mechanism of fatty-acid-dependent UCP1 uncoupling in brown fat mitochondria. Cell 151, 400–413.

Field F., Lee, S.B., Jan, Y.N., and Kirichok, Y. (2012). Activity of the mitochondrial calcium uniporter varies greatly between tissues. Nat. Commun. 3, 1317.

Flicker, D., Sancak, Y., Mick, E., Goldberger, O., and Mootha, V.K. (2019). Exploring the in vivo role of the mitochondrial calcium uniporter in brown fat bioenergetics. Cell Rep. 27, 1364–1375.e5.

Gherardi, G., Monticelli, H., Rizzuto, R., and Mammucari, C. (2020). The mitochondrial Ca<sup>2+</sup> uptake and the fine-tuning of aerobic metabolism. Front. Physiol. *11*, 554904.

Guo, X., Aviles, G., Liu, Y., Tian, R., Unger, B.A., Lin, Y.T., Wiita, A.P., Xu, K., Correia, M.A., and Kampmann, M. (2020). Mitochondrial stress is relayed to the cytosol by an OMA1-DELE1-HRI pathway. Nature *579*, 427–432.

Harms, M., and Seale, P. (2013). Brown and beige fat: development, function and therapeutic potential. Nat. Med. 19, 1252–1263.

Heaton, G.M., and Nicholls, D.G. (1977). The structural specificity of the nucleotide-binding site and the reversible nature of the inhibition of proton conductance induced by bound nucleotides in brown-adipose-tissue mitochondria. Biochem. Soc. Trans. *5*, 210–212.

Heaton, G.M., Wagenvoord, R.J., Kemp, A., Jr., and Nicholls, D.G. (1978). Brown-adipose-tissue mitochondria: photoaffinity labelling of the regulatory site of energy dissipation. Eur. J. Biochem. 82, 515–521.

Heymsfield, S.B., and Wadden, T.A. (2017). Mechanisms, pathophysiology, and management of obesity. N. Engl. J. Med. 376, 254–266.

Hoshino, A., Wang, W.J., Wada, S., McDermott-Roe, C., Evans, C.S., Gosis, B., Morley, M.P., Rathi, K.S., Li, J., Li, K., et al. (2019). The ADP/ATP translocase drives mitophagy independent of nucleotide exchange. Nature *575*, 375–379

Ikeda, K., Kang, Q., Yoneshiro, T., Camporez, J.P., Maki, H., Homma, M., Shinoda, K., Chen, Y., Lu, X., Maretich, P., et al. (2017). UCP1-independent signaling involving SERCA2b-mediated calcium cycling regulates beige fat thermogenesis and systemic glucose homeostasis. Nat. Med. *23*, 1454–1465.

Jing, Y., Niu, Y., Liu, C., Zen, K., and Li, D. (2018). In silico identification of lipid-binding alpha helices of uncoupling protein 1. Biomed. Rep. 9, 313–317.

Karpova, T., Danchuk, S., Kolobova, E., and Popov, K.M. (2003). Characterization of the isozymes of pyruvate dehydrogenase phosphatase: implications for the regulation of pyruvate dehydrogenase activity. Biochim. Biophys. Acta *1652*, 126–135.

Killian, J.A., Salemink, I., de Planque, M.R., Lindblom, G., Koeppe, R.E., 2nd, and Greathouse, D.V. (1996). Induction of nonbilayer structures in diacylphosphatidylcholine model membranes by transmembrane alpha-helical peptides: importance of hydrophobic mismatch and proposed role of tryptophans. Biochemistry *35*, 1037–1045.

Kwong, J.Q., Huo, J., Bround, M.J., Boyer, J.G., Schwanekamp, J.A., Ghazal, N., Maxwell, J.T., Jang, Y.C., Khuchua, Z., Shi, K., et al. (2018). The mitochondrial calcium uniporter underlies metabolic fuel preference in skeletal muscle. JCI Insight 3, e121689.

Lewis-Smith, D., Kamer, K.J., Griffin, H., Childs, A.M., Pysden, K., Titov, D., Duff, J., Pyle, A., Taylor, R.W., Yu-Wai-Man, P., et al. (2016). Homozygous deletion in MICU1 presenting with fatigue and lethargy in childhood. Neurol. Genet. 2, e59.

Logan, C.V., Szabadkai, G., Sharpe, J.A., Parry, D.A., Torelli, S., Childs, A.M., Kriek, M., Phadke, R., Johnson, C.A., Roberts, N.Y., et al. (2014). Loss-of-

function mutations in MICU1 cause a brain and muscle disorder linked to primary alterations in mitochondrial calcium signaling. Nat. Genet. 46, 188–193.

Lowell, B.B., and Spiegelman, B.M. (2000). Towards a molecular understanding of adaptive thermogenesis. Nature 404, 652–660.

Mallilankaraman, K., Doonan, P., Cárdenas, C., Chandramoorthy, H.C., Müller, M., Miller, R., Hoffman, N.E., Gandhirajan, R.K., Molgó, J., Birnbaum, M.J., et al. (2012). MICU1 is an essential gatekeeper for MCU-mediated mitochondrial Ca(2+) uptake that regulates cell survival. Cell *151*, 630–644.

Maus, M., Cuk, M., Patel, B., Lian, J., Ouimet, M., Kaufmann, U., Yang, J., Horvath, R., Hornig-Do, H.T., Chrzanowska-Lightowlers, Z.M., et al. (2017). Store-operated Ca<sup>2+</sup> entry controls induction of lipolysis and the transcriptional reprogramming to lipid metabolism. Cell Metab. *25*, 698–712.

Meng, Y., Xiang, R., Yan, H., Zhou, Y., Hu, Y., Yang, J., Zhou, Y., and Cui, Q. (2020). Transcriptomic landscape profiling of metformin-treated healthy mice: implication for potential hypertension risk when prophylactically used. J. Cell. Mol. Med. *24*, 8138–8150.

Murphy, E., Pan, X., Nguyen, T., Liu, J., Holmström, K.M., and Finkel, T. (2014). Unresolved questions from the analysis of mice lacking MCU expression. Biochem. Biophys. Res. Commun. *449*, 384–385.

Ng, M., Fleming, T., Robinson, M., Thomson, B., Graetz, N., Margono, C., Mullany, E.C., Biryukov, S., Abbafati, C., Abera, S.F., et al. (2014). Global, regional, and national prevalence of overweight and obesity in children and adults during 1980–2013: a systematic analysis for the Global Burden of Disease Study 2013. Lancet *384*, 766–781.

Nguyen, N.X., Armache, J.P., Lee, C., Yang, Y., Zeng, W., Mootha, V.K., Cheng, Y., Bai, X.C., and Jiang, Y. (2018). Cryo-EM structure of a fungal mitochondrial calcium uniporter. Nature *559*, 570–574.

Odegaard, J.I., Lee, M.W., Sogawa, Y., Bertholet, A.M., Locksley, R.M., Weinberg, D.E., Kirichok, Y., Deo, R.C., and Chawla, A. (2016). Perinatal licensing of thermogenesis by IL-33 and ST2. Cell *166*, 841–854.

Pan, X., Liu, J., Nguyen, T., Liu, C., Sun, J., Teng, Y., Fergusson, M.M., Rovira, I.I., Allen, M., Springer, D.A., et al. (2013). The physiological role of mitochondrial calcium revealed by mice lacking the mitochondrial calcium uniporter. Nat. Cell Biol. *15*, 1464–1472.

Perocchi, F., Gohil, V.M., Girgis, H.S., Bao, X.R., McCombs, J.E., Palmer, A.E., and Mootha, V.K. (2010). MICU1 encodes a mitochondrial EF hand protein required for Ca(2+) uptake. Nature *467*, 291–296.

Pettitt, S.J., Liang, Q., Rairdan, X.Y., Moran, J.L., Prosser, H.M., Beier, D.R., Lloyd, K.C., Bradley, A., and Skarnes, W.C. (2009). Agouti C57BL/6N embryonic stem cells for mouse genetic resources. Nat. Methods *6*, 493–495.

Platt, R.J., Chen, S., Zhou, Y., Yim, M.J., Swiech, L., Kempton, H.R., Dahlman, J.E., Parnas, O., Eisenhaure, T.M., Jovanovic, M., et al. (2014). CRISPR-Cas9 knockin mice for genome editing and cancer modeling. Cell *159*, 440–455.

Sancak, Y., Markhard, A.L., Kitami, T., Kovács-Bogdán, E., Kamer, K.J., Udeshi, N.D., Carr, S.A., Chaudhuri, D., Clapham, D.E., Li, A.A., et al. (2013). EMRE is an essential component of the mitochondrial calcium uniporter complex. Science *342*, 1379–1382.

Schreiber, R., Diwoky, C., Schoiswohl, G., Feiler, U., Wongsiriroj, N., Abdellatif, M., Kolb, D., Hoeks, J., Kershaw, E.E., Sedej, S., et al. (2017). Cold-induced thermogenesis depends on ATGL-mediated lipolysis in cardiac muscle, but not brown adipose tissue. Cell Metab. *26*, 753–763.e7.

Shabalina, I.G., Petrovic, N., de Jong, J.M., Kalinovich, A.V., Cannon, B., and Nedergaard, J. (2013). UCP1 in brite/beige adipose tissue mitochondria is functionally thermogenic. Cell Rep. 5, 1196–1203.

Shi, M., Huang, X.Y., Ren, X.Y., Wei, X.Y., Ma, Y., Lin, Z.Z., Liu, D.T., Song, L., Zhao, T.J., Li, G., et al. (2021). AIDA directly connects sympathetic innervation to adaptive thermogenesis by UCP1. Nat. Cell Biol. 23, 268–277.

Shin, H., Ma, Y., Chanturiya, T., Cao, Q., Wang, Y., Kadegowda, A.K.G., Jackson, R., Rumore, D., Xue, B., Shi, H., et al. (2017). Lipolysis in brown adipocytes is not essential for cold-induced thermogenesis in mice. Cell Metab. 26, 764–777.e5.

Skarnes, W.C., Rosen, B., West, A.P., Koutsourakis, M., Bushell, W., Iyer, V., Mujica, A.O., Thomas, M., Harrow, J., Cox, T., et al. (2011). A conditional knoc

# **Article**



e15545kout resource for the genome-wide study of mouse gene function. Nature 474, 337-342.

Slot, J.W., and Geuze, H.J. (2007). Cryosectioning and immunolabeling. Nat. Protoc. 2, 2480-2491.

Taylor, E.B. (2017). Functional properties of the mitochondrial carrier system. Trends Cell Biol. 27, 633-644.

Tsai, M.F., Phillips, C.B., Ranaghan, M., Tsai, C.W., Wu, Y., Williams, C., and Miller, C. (2016). Dual functions of a small regulatory subunit in the mitochondrial calcium uniporter complex. eLife 5, e15545.

Wang, W., and Seale, P. (2016). Control of brown and beige fat development. Nat. Rev. Mol. Cell Biol. 17, 691-702.

Wang, G., Meyer, J.G., Cai, W., Softic, S., Li, M.E., Verdin, E., Newgard, C., Schilling, B., and Kahn, C.R. (2019). Regulation of UCP1 and mitochondrial metabolism in brown adipose tissue by reversible succinylation. Mol. Cell 74, 844-857.e7.

Wang, P., Loh, K.H., Wu, M., Morgan, D.A., Schneeberger, M., Yu, X., Chi, J., Kosse, C., Kim, D., Rahmouni, K., et al. (2020). A leptin-BDNF pathway regulating sympathetic innervation of adipose tissue. Nature 583, 839-844.

Wittig, I., Braun, H.P., and Schägger, H. (2006). Blue native PAGE. Nat. Protoc. 1, 418-428.

Zhuo, W., Zhou, H., Guo, R., Yi, J., Zhang, L., Yu, L., Sui, Y., Zeng, W., Wang, P., and Yang, M. (2021). Structure of intact human MCU supercomplex with the auxiliary MICU subunits. Protein Cell 12, 220-229.





# **STAR**\***METHODS**

# **KEY RESOURCES TABLE**

REAGENT or RESOURCE	SOURCE	IDENTIFIER
Antibodies		
Rabbit anti-UCP1	Sigma-Aldrich	Cat. #U6382; RRID: AB_261838
Mouse anti-HSP90α/β	Santa Cruz Biotech.	Cat. #sc-7947; RRID: AB_2121235
Rabbit anti-EMRE	Santa Cruz Biotech.	Cat. #sc-86337; RRID: AB_2250685
Rabbit anti-MCU	Cell Signaling	Cat. #14997; RRID: AB_2721812
Rabbit anti-MICU1	Sigma	Cat. #HPA037479; RRID: AB_2675495
Mouse anti-SDHB	Santa Cruz Biotech.	Cat. #sc-271548; RRID: AB_10659104
Mouse anti-FLAG	Abmart	Cat. #293881
Mouse anti-PDHE1α	Santa Cruz Biotech.	Cat.#sc-377092; RRID: AB_2716767
Rabbit anti-phospho-PDHE1α <sup>S293</sup>	Millipore	Cat.#ABS204; RRID: AB_11205754
Rabbit anti-AKT	Cell Signaling	Cat. #9272; RRID: AB_329827
Rabbit anti-phospho-AKT (Ser473)	Cell Signaling	Cat. #9271; RRID: AB_329825
Mouse anti-NDUFS1	Abcam	Cat. #ab22094; RRID: AB_2151098
Rabbit anti-HA	Cell Signaling	Cat. #3724; RRID: AB_1549585
Goat anti-mouse IgG:HRP	Thermo Scientific	Cat. #32430; RRID: AB_1185566
Goat anti-rabbit IgG:HRP	Thermo Scientific	Cat. #31460; RRID: AB_228341
Alexa Fluor 488-labelled goat anti-mouse secondary antibody	Invitrogen	Cat. #A11029; RRID: AB_138404
Alexa Fluor 647-labelled goat anti-rabbit secondary antibody	Invitrogen	Cat. #A21244; RRID: AB_2535812
Chemicals, peptides, and recombinant proteins		
Acrylamide	Sigma-Aldrich	Cat. #V900845
Anti-DYKDDDDK affinity beads	Smart-Lifescience	Cat. #SA042001
Anti-HA magnetic beads	Thermo scientific	Cat. #88836
Atglistatin	MCE	Cat. #HY-15859
Bisacrylamide	Sigma-Aldrich	Cat. #V900301
Bovine Serum Albumin (fatty-acid free)	Yuanye Biotech.	Cat. #S25762
CAY10499	Cayman chemical	Cat. #10007875
CL-316,243	Sigma-Aldrich	Cat. #C5976
Collagenase Type I	Sigma-Aldrich	Cat. #V900891
Collagenase Type II	Sigma-Aldrich	Cat. #V900892
D-desthiobiotin	IBA	Cat. #2-1000-005
Dexamethasone	Sigma-Aldrich	Cat. #D4902
Diamide	Santa-cruz	Cat. #sc-211289
Digitonin	Biosynth	Cat. #D3200
FCCP	MCE	Cat. #HY-100410
Fluo8-AM	AAT Bioquest	Cat. #21080
GDP disodium salt	Abcam	Cat. #ab146529
HEPES	Sigma-Aldrich	Cat. #V900477
H89	Sigma-Aldrich	Cat. #B1427
BMX	Sigma-Aldrich	Cat. #I5879
ndomethacin	Sigma-Aldrich	Cat. #I8280
NAC	Sigma-Aldrich	Cat. #A7250
	<u> </u>	
Norepinephrine	Sigma-Aldrich	Cat. #N5785

(Continued on next page)





Continued		
REAGENT or RESOURCE	SOURCE	IDENTIFIER
Rosiglitazone	Sigma-Aldrich	Cat. #R2408
Rotenone	Sigma-Aldrich	Cat. #R8875
rProtein A/G Beads	Smart-Lifesciences	Cat. #SA032005
Streptactin Beads 4FF	Smart-Lifescience	Cat. #SA053005
SDS	Sigma-Aldrich	Cat. #V900859
Sodium pyruvate solution	Sigma-Aldrich	Cat. #S8636
Streptactin Beads 4FF	Smart-Lifescience	Cat. #SA05301L
Т3	Sigma-Aldrich	Cat. #T2877
TRIzol Reagent	Invitrogen	Cat. #T9424
3-isobutyl-1-methylxanthine	Sigma-Aldrich	Cat. #I5879
2,2,2-Tribromoethanol	Sigma-Aldrich	Cat. #T48402
Critical commercial assays		
5× All-In-One RT MasterMix	abm	Cat. #G492
2× qPCR MasterMix-ROX	abm	Cat. #MasterMix-R
BCA Protein Assay Kit	Cwbiotech	Cat. #CW0014S
Deposited data		
Original western blot images and raw data	This paper	Data S1
Experimental models: Cell lines		
HEK 293T	ATCC	Cat. #ATCC CRL-3216; RRID: CVCL_0063
Experimental models: Organisms/strains		
Mouse: Ucp1 <sup>Cre</sup>	The Jackson Laboratory	Stock No. 024670
Mouse: Adiponectin <sup>Cre</sup>	The Jackson Laboratory	Stock No. 010803
Mouse: Rosa26-LSL-Cas9 knock-in	The Jackson Laboratory	Stock No. 026175
Mouse: ob/+	The Jackson Laboratory	Stock No. 000632
Mouse: C57BL/6J	The Jackson Laboratory	Stock No. 000664
Mouse: C57BL/6N-Mcu <sup>tm1c(EUCOMM)Hmgu</sup> /H	European Mouse Mutant Archive	Stock No. HEPD0762_7_B01
Oligonucleotides		
qPCR primers	This paper	Table S2
sgRNA targeting sequence: EMRE #1 GGCGAT GTCTACACCGTACC	This paper	N/A
sgRNA targeting sequence: MICU1 #1 CTAGTT CTGCCAACGCAGAA	This paper	N/A
Recombinant DNA		
Plasmid: pAAV-ADP-MCS-Strep/FLAG/HA	This paper	N/A
Plasmid: pAAV-U6-sgRNA-mCherry	This paper	N/A
Software and algorithms		
GraphPad Prism 8	GraphPad Software	https://www.graphpad.com/scientific-software/prism/
ImageJ	NIH	https://imagej.nih.gov/ij/
Volocity	PerkinElmer	http://www.perkinelmer.com/cellularimagingsupport
Other		
60% high fat diet	Research Diets	D12492
J 2000		

# **RESOURCE AVAILABILITY**

# **Lead contact**

Further information and requests for resources and reagents should be directed to and will be fulfilled by the lead contact, Yifu Qiu (yifu.qiu@pku.edu.cn).





# **Materials availability**

This study did not generate new unique reagents. All other data and materials that support the findings of this study are available within the article and supplemental information or available from the authors upon request.

## Data and code availability

Original western blot images and all raw data used to create the graphs can be found in Data S1. This paper does not report any original code. Any additional information required to reanalyze the data reported in this paper is available from the lead contact upon request.

#### **EXPERIMENTAL MODEL AND SUBJECT DETAILS**

#### **Animal models**

*Ucp1*<sup>Cre</sup> (024670), *Adiponectin*<sup>Cre</sup> (010803), *Rosa26-LSL-Cas9* knock-in (026175) and *ob/*+ (000632) mice were obtained from The Jackson Laboratory. All the above strains are on a C57BL6/J background. The *Mcu*<sup>f/f</sup> (*C57BL/6N-Mcu*<sup>tm1c(EUCOMM)Hmgu</sup>/H) mice were obtained from the MRC-Harwell which distributes these mice on behalf of the European Mouse Mutant Archive (Bradley et al., 2012; Pettitt et al., 2009; Skarnes et al., 2011), and crossed with *Ucp1*<sup>Cre</sup> (C57BL6/J background) mice to generate *Mcu*<sup>f/f</sup> *Ucp1*<sup>Cre</sup> (selected for *Nnt*<sup>mut</sup>) mice.

Emre-BKO and Micu1-BKO mice were generated by CRISPR-Cas9-mediated genome editing (Platt et al., 2014). In brief, the AAVs expressing the Cas9-gRNA for Emre (GGC GAT GTC TAC ACC GTA CC) or Micu1 (CTA GTT CTG CCA ACG CAG AA) were injected into the BAT of Rosa26-LSL-Cas9; Adiponectin Cre mice to knock out Emre or Micu1 specifically in BAT.

All mouse experiments were performed according to PKU IACUC guidelines. Unless otherwise specified, mice were housed at 22°C and under a 12-h light/dark cycle with libitum access to food and water. Sex- and age-matched mice (8-12 weeks) were used for in vivo studies. Mice were used for AAV injection at the age of 6 weeks.

#### **Primary cell culture**

#### Isolation and differentiation of primary preadipocytes

Stromal vascular fraction (SVF) of BAT was isolated from 2-week old WT mice. Interscapular BAT was minced and digested in collagenase I (2 mg/ml) contained SVF buffer (1.1 mM CaCl $_2$ , 118 mM NaCl, 2.7 mM KCl, 0.4 mM NaH $_2$ PO $_4$ , 0.5 mM MgCl $_2$ , 5.5 mM Glucose, 20 mM HEPES, 1% BSA (fatty-acid free)) at 37°C for 60 min (120 rpm). The digestion was ended with a volume SVF buffer addition and the cell suspension was centrifuged at 1000 rpm for 5 minutes. The pelleted cells were re-suspended with SVF buffer and filtered through a 75- $\mu$ m cell strainer. Then the SVF cells were plated on 6-cm dish in DMEM supplemented with 10% FBS, 20 mM HEPES at 37°C in a humidified 5% CO $_2$  incubator. Once cells reached confluence, cell medium was replaced by the induction medium for brown adipocyte differentiation (5  $\mu$ g/ml insulin, 1 nM T3, 125  $\mu$ M indomethacin, 1  $\mu$ g/ml Dexamethosone, 0.5 mM 3-isobutyl-1-methylxantine and 0.5  $\mu$ M Rosiglitazone) for 48 hours. The medium was then changed to maintenance medium (5  $\mu$ g/ml insulin, 1 nM T3 and 0.5  $\mu$ M Rosiglitazone). After 7-8 days, mature brown adipocytes were used for co-IP experiments.

# Isolation of primary mature brown adipocytes

Mature brown adipocytes from BAT were isolated as previously described with minor modifications (Chen et al., 2017). Briefly, the interscapular BAT was minced and digested in HBSS (Corning, 21-023-CV) with 4% fatty-acid free BSA and 2 mg/mL collagenase II (Vetec, V900892) for 30 min at 37°C (100 rpm). Cells were washed for three times with Krebs Ringer bicarbonate-modified buffer (KRBMB, 120 mM NaCl, 5 mM KCl, 1 mM MgCl<sub>2</sub>, 1 mM CaCal<sub>2</sub>, 0.4 mM K<sub>2</sub>HPO<sub>4</sub>, 10mM Glucose, 15 mM NaHCO<sub>3</sub> and 20 mM HEPES) supplemented with 4% fatty-acid free BSA. Supernatant mature brown adipocytes were collected by centrifugation at 30 g for 5 min. Freshly isolated mature brown adipocytes were suspended in aerated culture media (DMEM/F-12, Hyclone, plus 10% FBS) in glass bottom cell culture dish (NEST, 801002) coated with type IV collagen. The dish was filled up with culture media, covered with lid to avoid bubbles and turned the dish upside down to allow attachment for more than 12 h at 37°C in a humidified 5% CO<sub>2</sub> incubator. The attached cells on the glass bottom were used for calcium-imaging or immunofluorescence staining analysis on the next day.

# **METHOD DETAILS**

# Western blot

Tissues were lysed in modified RIPA buffer (450 mM NaCl, 1% NP-40, 0.1% SDS, 0.5% Deoxycholic acid (sodium salt), 50 mM Tris pH 7.5, 1x complete protease inhibitor). Total cellular protein ( $30 \mu g$ ) was separated on SDS-PAGE gels and transferred to nitrocellulose membrane. After blocking in 5% defatted milk, membranes were incubated in primary antibody at  $4^{\circ}$ C overnight. The primary antibodies used in this study were: rabbit anti-UCP1 (Abcam, ab10983, 1:40,000 for BAT, 1:2000 for co-IP experiments), rabbit anti-EMRE (Santa Cruz Biotech, sc-86337, 1:300), rabbit anti-MCU (Cell Signaling Technologies, 14997, 1:2000), rabbit anti-HA (Cell Signaling Technologies, 3724, 1:2000), mouse anti-SDHB (Santa Cruz Biotech, sc-271548, 1:2000), mouse anti-FLAG (Abmart, 314375, 1:5000), mouse anti-PDHE1 $\alpha$  (Santa Cruz Biotech, sc-377092, 1:5000), rabbit anti-phospho-PDHE1 $\alpha$  (Millipore, ABS204, 1:2000), rabbit anti-AKT (Cell Signaling Technologies, 9271, 1:2000), mouse anti-HSP90 $\alpha/\beta$  (Santa Cruz Biotech, sc13119, 1:10000), mouse





anti-NDUFS1 (Abcam, ab22094, 1:10000). The membranes were then incubated in HRP-conjugated secondary antibodies at 37°C for 1 h and visualized using Tanon 5200 Chemiluminescent Imaging System.

### Gene expression analysis

Total RNA was extracted from frozen tissues using TRIzol (Invitrogen). Reverse transcription was carried out using MasterMix (Abm), and quantitative PCR reactions were performed in a 96-well format using a StepOnePlus Real-time PCR system (Applied Biosystems). Normalized mRNA expression was calculated using the  $\Delta\Delta$ Ct method, using 36B4 mRNA as the reference gene.

#### Measurement of core body temperature

For fasting-cold experiments, mice were first fasted at 22°C for 5 h and then transferred to new pre-chilled cages at 4°C. The mice were single-housed with free access to water. Core body temperatures were monitored at various time points using a mouse rectal probe (RET3, World Precision Instruments).

# Measurement of BAT temperature with implanted probe

*Mcu*<sup>f/f</sup> and *Mcu*<sup>f/f</sup>*Ucp1*<sup>Cre</sup> mice were implanted with temperature probes 2 weeks prior to fasting-cold experiments. In brief, mice were anaesthetized and the telemetric sensor (TTA-XS, Stellar Telemetry, TSE Systems) was subcutaneously implanted above the interscapular BAT. Telemetric data were acquired using VitalView software.

## Infrared thermographic imaging

For whole-body infrared thermographic imaging, after fasting-cold challenge, mice were anaesthetized and laid side by side to acquire comparative infrared images with a FLIR T530 infrared camera (FLIR Systems). To quantify interscapular region temperature, the average surface temperature from a region of the interscapular BAT was taken with FLIR Tools Desktop software v5.13.18031.2002.

#### **Energy expenditure and body composition measurements**

For measuring thermogenic capacity of BAT, mice were anesthetized, and baseline and NE (1 mg/kg) or CL-316,243 (1 mg/kg)-induced O<sub>2</sub> consumptions were monitored at 32°C in a Comprehensive Lab Animal Monitoring System (CLAMS, Columbus Instruments) chamber. NE or CL-316,243 was locally injected into the BAT of anesthetized mice. Fat oxidation was calculated using the formula: calories of fat consumed=heat\*(1-RER)/0.293, in which the RER represents the respiratory exchange ratio (http://www.colinst.com, equations for energy expenditure). For measuring energy expenditure of mice fed HFD, VO<sub>2</sub>, food intake and total locomotor activity were recorded in the CLAMS chamber. Prior to experiments, mice were acclimated in the chamber for 24 h. Fat mass and lean mass were measured by Dual-energy X-ray absorptiometry (DXA).

# **Isolation of BAT mitochondria**

BAT mitochondria were isolated using the previously described method with minor modifications (Odegaard et al., 2016). Briefly, interscapular BAT was minced and homogenized with a Dounce glass tissue homogenizer in isolating buffer (250 mM sucrose, 10 mM HEPES, 1 mM EGTA, and 0.3% BSA, pH 7.2). The homogenate was centrifuged at 8,500 g for 10 min at 4°C. The resuspended mitochondrial pellet was homogenized again and centrifuged at 600 g for 10 min at 4°C. The supernatant was centrifuged at 8,500 g for 10 min at 4°C to pellet the mitochondria that were ready for use.

# **Oxygen consumption**

Mitochondrial oxygen consumption was measured with a Clark-type oxygen electrode as previously described (Shabalina et al., 2013) (Model 782/MT200, Strathkelvin Instruments, Scotland). Briefly, freshly isolated BAT mitochondria (about 0.5 mg mitochondrial protein per mouse per reaction) were suspended in mitochondrial respiratory buffer (75 mM sucrose, 10 mM KCl, 10 mM Tris-HCl, 5 mM KH $_2$ PO4, 225 mM mannitol and 0.1% fatty acid-free BSA, pH 7.2). The total respiration was measured in the presence of 5 mM pyruvate and 3 mM malate. The UCP1-dependent respiration was estimated as the respiration that was inhibited by 2 mM GDP, and the residual respiration was regarded as UCP1-independent one. The following addition of 1.4  $\mu$ M FCCP triggered the maximal respiration.

# **Construct design and site-directed mutagenesis**

The open reading frames (ORFs) of mouse *Mcu*, *Emre*, *Micu1*, *Ucp1*, *Sdhb* and *Ant1* were cloned from BAT cDNA. All the above ORFs were cloned into the vector pAAV-ADP (1.6 kb *Adiponectin* promoter)-MCS-HA/FLAG/Strep for AAV (2/8) packaging.





GAC AAA-3'; mutagenesis primers for EMRE (S85W); forward, 5'-GTC GGG ACA CTC ATC TGG AAG AAC TTC-3'; reverse, 5'-AGC AGC GAA GTT CTT CCA GAT GAG TGT-3'; linked EMRE-UCP1 was constructed by linking the C terminus of EMRE and the N terminus of UCP1 with a 21-amino acid linker.

#### **AAV** injection into BAT

Mice were anesthetized with tribromoethanol (Avertin, Sigma-Aldrich), and the hair above the interscapular area was removed and followed by a surgical scrub with lodophors. A small cut was made on the skin to expose the interscapular BAT, and AAVs were slowly injected into each lobe of the BAT with five needle points for each lobe and 5  $\mu$ l per point (finally  $5 \times 10^{11}$  AAV particles per mouse). The skin was closed with surgical pins followed by several injections of analgesics. Experiments were performed 3 weeks post injection.

### Strep purification followed by mass spectrometry (MS)

WT mice were locally injected in BAT with ADP-MCU-Strep-3×FLAG-Strep or ADP-SDHB-Strep-3×FLAG-Strep AAV. Two weeks post injection, mice housed at 22°C were shifted to 4°C environment and housed for 1 week. Next, BAT mitochondria were isolated and solubilized in solubilization buffer (1% [w/v] digitonin, 50 mM Tris-HCl, pH 7.5, 1 mM EDTA, 150 mM NaCl, 1 x complete protease inhibitor) for 45 min at 4°C. The mitochondrial lysate was cleared by centrifugation at 40,000 g at 4°C for 30 min and diluted in solubilization buffer to a final digitonin concentration of 0.5%. The cleared lysate was incubated with Streptactin Beads 4FF (Smart-Lifescience) for 2 h at 4°C. Beads were washed 3 times with washing buffer (0.1% [w/v] digitonin, 50 mM Tris-HCl, pH 7.5, 1 mM EDTA, 150 mM NaCl, 1x complete protease inhibitor). Bound protein was eluted with eluting buffer (5 mM D-desthiobiotin (IBA), 50 mM Tris-HCl, pH 7.5, 1 mM EDTA, 150 mM NaCl, 1 x complete protease inhibitor). Eluted protein was concentrated using 100-kDa cutoff concentrator (Millipore), and then separated by SDS-PAGE followed by silver staining. The interested bands were cut and sent for MS analysis in Proteinomics Facility at Technology Center for Protein Sciences, Tsinghua University.

# Co-immunoprecipitation (co-IP)

Co-IP experiments were performed as a previously described protocol with minor modifications (Hoshino et al., 2019). Freshly isolated BAT mitochondria were solubilized in solubilization buffer (1% [w/v] digitonin, 50 mM Tris-HCl, pH 7.5, 1 mM EDTA, 150 mM NaCl, 1×complete protease inhibitor) for 30 min at 4°C. About 0.5 mg BAT mitochondrial protein per mouse was solubilized in 100 μl solubilization buffer. The mitochondrial lysate was cleared by centrifugation at 20,000g at 4°C for 30 min and diluted in solubilization buffer to a final digitonin concentration of 0.5%. The cleared lysate was incubated with anti-HA Magnetic Beads (Thermo Fisher Science) or FLAG antibody conjugated beads (Smart-Lifescience) for 2 h at 4°C. Beads were washed 3 times with washing buffer (0.1% [w/v] digitonin, 50 mM Tris-HCl, pH 7.5, 1 mM EDTA, 150 mM NaCl, 1xcomplete protease inhibitor). Bound protein was eluted with sample buffer (62.5 mM Tris-HCl, pH 6.8, 2% SDS, 5% glycerol, 0.017% Bromophenol blue, 50 mM DTT), and then separated by SDS-PAGE.

# **Blue native PAGE**

Sample preparation and electrophoresis for blue native PAGE were performed according to a previously described protocol (Wittig et al., 2006). Briefly, the purified protein samples in lysis buffer (150 mM NaCl, 50 mM Tris-HCl, pH 7.5, 1 mM EDTA, 0.1% digitonin) were added with 5% glycerol and Coomassie blue G-250 dye at a detergent/dye ratio of 8 (gram/gram). 4%-20% acrylamide gradient gels were used, the electrode buffers were precooled to 4°C before use, and electrophoresis was performed at 4°C. Gels were running at 100 V for 1 h with Dark Blue Cathode Buffer, and then at 200-250 V for 1 h with Light Blue Cathode Buffer. Once electrophoresis was completed, protein was transferred to a PVDF membrane and detected by immunoblot.

### Immuno-electronmicroscopy (IEM)

For IEM, sample preparation was performed according to the procedures described previously (Slot and Geuze, 2007). Briefly, fresh brown adipose tissue was immediately immersed in 0.1 M phosphate buffer (pH 7.4) containing 4% PFA/0.25% glutaraldehyde (GA), dissected into 2 mm<sup>3</sup> blocks, incubated for 2 h at room temperature, and then held in 2% PFA overnight at 4°C. For quenching free aldehyde, tissue blocks were washed with 150 mM glycine two times for 5 min each, then rinsed two times with phosphate buffer for 5 min each. Samples were incubated in gelatin (PanReac AppliChem, 147116.1210) series (2%, 5% and 2x 12%) for 30 min each at 37°C, and then were cut into 0.5 mm3 cubic blocks. Gelatin blocks were transferred into 2.3 M sucrose and rotated at 4°C overnight. Blocks were glued on an aluminum pin and frozen in liquid nitrogen. Frozen blocks were trimmed at -80°C and cut into 70 nm at -120°C using a Leica FC7 cryo-ultramicrotome. Cryosections were mounted on 100-mesh formvar/carbon-coated nickel grids. For single labelling, the grids were incubated with UCP1 antibody (Abcam, ab10983, 1:10) or FLAG antibody (Proteintech, 20543-1-AP, 1:10) or HSP60 (Abcam, ab46798, 1:10). After washing with PBS, secondary antibody (15-nm, 10-nm or 5-nm protein A-gold [Cell Microscopy Center, University Medical Center Utrecht, Utrecht, The Netherlands]) was incubated for 30 min. After labeling, sections were treated with 1% GA and embedded in a mixture of 2% methylcellulose/2%uranyl acetate (9:1). Cryosections were analyzed at 120 kV on a Tecnai G2 Spirit (FEI) transmission electron microscope equipped with a CMOS camera (PHURONA, EMSIS).

# Measurement of NE-induced mitochondrial calcium uptake in primary mature brown adipocytes

To monitor mitochondrial calcium uptake, we constructed AAV expressing GCaMP5-mt and injected mouse BAT. Cytosolic calcium was monitored using Fluo8-AM. Primary mature brown adipocytes were isolated from the injected BAT, and imaged in HBSS+20 mM

# Article



glucose. After NE or isoproterenol (iso) (1.5 µM) treatment, a series of images were captured every second by DeltaVision Elite microscopy (Applied Precision) using 561 nm laser excitation with a Plan Fluor 10x air inversion objective and data acquisition software SoftWoRx. Fluorescence was acquired at 488 nm. Imaging data were processed using Volocity. After subtracting background fluorescence, GCaMP5-mt intensity was quantified within an ROI for each cell over the 720-sec imaging period.

#### **Immunofluorescence**

Immunofluorescence experiments were performed as a previously described protocol with minor modifications (Guo et al., 2020). Primary mature brown adipocytes were isolated from BAT expressing MICU1-FLAG, MCU-FLAG, EMRE-FLAG and EMRE-UCP1-HA respectively, and attached to the glass bottom cell culture dish as described above. After PBS wash, cells were fixed with 4% (w/v) paraformaldehyde and 0.1% (w/v) glutaraldehyde in PBS for 30 min. Cells were then permeabilized and blocked in a blocking buffer (3% w/v BSA and 0.1% v/v Triton X-100 in PBS) for 1 h. Next, the cells were incubated with primary FLAG antibody (Abmart, 314375, 1:200) or HA antibody (Cell Signaling Technologies, 3724, 1:200) in blocking buffer for 12 h at 4°C. The cells were washed with washing buffer (0.3% w/v BSA and 0.01% v/v Triton X-100 in PBS) for three times, and then incubated with dye-labelled secondary antibody (Alexa Fluor 488-labelled goat anti-mouse, Invitrogen, A11029, 1:400; Alexa Fluor 647-labelled goat anti-rabbit, Invitrogen, A21244, 1:400) for 1 h at room temperature. Then, the samples were washed three times and mounted with mounting medium. The bottom glass slip was sealed to the glass slide with nail polish and stored at 4°C, avoiding exposure to light. The samples were imaged by DeltaVision OMX SR-3D-SIM (Applied Precision) using 488 nm laser excitation with a 60x oil immersion objective and data acquisition software SoftWoRx. Imaging data were processed using ImageJ.

# NADH production in isolated primary mature brown adipocytes

To assess mitochondrial NADH production, 150,000 freshly isolated primary mature brown adipocytes were suspended in Tyrode's buffer (150 mM NaCl, 5.4 mM KCl, 2 mM CaCl<sub>2</sub>, 5 mM HEPES, 10 mM glucose, 2 mM sodium pyruvate at pH 7.4). NADH autofluorescence was read at 350ex/460em using a Spectrofluorophotometer (RF-5301PC). The basal NADH autofluorescence was measured in the presence of 3 mM malate, brown adipocytes were gently stirred and 10 μM NE was added followed by 2 μM

## Intraperitoneal insulin tolerance test and glucose tolerance test

For insulin tolerance test, mice fed HFD for 12 weeks were fasted for 6 h. Insulin (1 U per kg body weight) was administered i.p., and blood glucose levels were measured from the tail at 0, 15, 30, 60 and 120 min using a glucometer. For glucose tolerance test, mice fed HFD for 14 weeks were fasted for 14 h. Glucose (2 g per kg body weight) was administered i.p., and blood glucose levels were measured from the tail without use of restraint at 0, 15, 30, 60 and 120 min using a glucometer.

# **Insulin sensitivity**

Mice fed HFD for 16 weeks were fasted for 6 h. Insulin (1 U per kg body weight) was administered i.p., and tissues (BAT, scWAT, eWAT, liver, muscle) were harvested and snap frozen in liquid nitrogen 15 min after injection of insulin. Assessment of insulin sensitivity of metabolic tissues was measured as phosphorylation levels of AKT at S473 normalized to total AKT.

# Tissue hematoxylin and eosin (H&E) staining

BAT tissues were fixed in 4% paraformaldehyde. Paraffin-embedding, sectioning and H&E staining were performed by the pathology core facility of Institute of Molecular Medicine, Peking University.

# **QUANTIFICATION AND STATISTICAL ANALYSIS**

Data are presented as mean ± SEM and analyzed using GraphPad Prism. To determine statistical differences, unpaired two-tailed Student's t test was applied for single-variable and two-group comparison; one-way ANOVA followed by Bonferroni posttests for single-variable and multiple-group comparison; two-way ANOVA followed by Bonferroni posttests for two-variable and multiplegroup comparison. Significance was considered as \*p < 0.05; \*\*p < 0.01; \*\*\*p < 0.001; \*\*\*\*p < 0.0001; n.s.,  $p \ge 0.05$ .